NACA

RESEARCH MEMORANDUM

INVESTIGATION AT SUPERSONIC AND SUBSONIC MACH NUMBERS

OF AUXILIARY INLETS SUPPLYING SECONDARY AIR FLOW

TO EJECTOR EXHAUST NOZZLES

By Donald P. Hearth and Robert W. Cubbison

Lewis Flight Propulsion Laboratory
Cleveland, Ohio

CLASSIFIED DOCUMENT

This material contains information affecting the National Defense of the United States within the meaning of the espionage laws, Title 18, U.S.C., Secs. 793 and 794, the transmission or revelation of which in any manner to an unauthorized person is prohibited by law.

NATIONAL ADVISORY COMMITTEE
FOR AERONAUTICS

WASHINGTON
January 25, 1956

3809

CM-1

NATIONAL ADVISORY COMMITTEE FOR AERONAUTICS

RESEARCH MEMORANDUM

INVESTIGATION AT SUPERSONIC AND SUBSONIC MACH NUMBERS OF AUXILIARY

INLETS SUPPLYING SECONDARY AIR FLOW TO EJECTOR EXHAUST NOZZLES

By Donald P. Hearth and Robert W. Cubbison

SUMMARY

An investigation was conducted on several auxiliary inlets supply-
ing secondary air flow to ejector exhaust nozzles. The inlets were
located in a fuselage boundary layer and were evaluated in conjunction
with two ejector configurations. The tests were conducted over a wide
range of primary nozzle pressure ratios at free-stream Mach numbers of
0.64, 1.5, 1.8, and 2.0.

The results indicated increases in auxiliary-inlet pressure recov-
ery with increases in scoop height relative to the boundary-layer thick-
ness. The pressure recovery increased at about the same rate as theo-
retically predicted for an inlet in a boundary layer having a one-seventh
power profile but was only about 0.68 to 0.75 of the theoretically ob-
tainable values. Under some operating conditions, flow from the primary
jet was exhausted through the auxiliary inlet. This phenomenon could
be predicted from the ejector pumping characteristics.

INTRODUCTION

Increases beyond the jet thrust of a conventional convergent nozzle
have been demonstrated when air taken aboard for cooling purposes is
pumped through an ejector surrounding the primary nozzle. This second-
ary air flow may be supplied by auxiliary type inlets such as reported
in references 1 to 3. In order to use this auxiliary air most efficient-
ly the air-supply characteristics should be properly matched to the
secondary air-flow requirements. A method for matching auxiliary inlets
with the secondary air-flow requirements of ejector exhaust nozzles has
been discussed in reference 4.

In the Lewis 8- by 6-foot supersonic wind tunnel, an experimental
program was conducted in order to obtain the performance of several dif-
ferent auxiliary-inlet configurations, to simultaneously confirm the
theoretical match points, and to evaluate the problems associated with

combining such inlets with ejectors. Several auxiliary inlet-ejector configurations were investigated at free-stream Mach numbers of 0.64, 1.5, 1.8, and 2.0 over a wide pressure-ratio range. The results of this program are reported herein.

SYMBOLS

The following symbols are used in this report:

A area, sq ft

A_m cross-sectional area of body, 0.379 sq ft

C_D drag coefficient, $\dfrac{\text{Drag}}{\frac{1}{2}\rho_0 V_0^2 A_m}$

C_p inlet cowl-pressure coefficient, $\dfrac{p - p_0}{\frac{1}{2}\rho_0 V_0^2}$

D diameter, ft

$\dfrac{D_s}{D_p}$ ejector diameter ratio

H length of inlet cowl, ft

h height of auxiliary inlet cowl lip from fuselage, in.

l distance from start of primary nozzle, in.

L total length of auxiliary inlet-ejector system, 2.029 ft

M Mach number

$\dfrac{m_s}{m_0}$ auxiliary-inlet mass-flow ratio

P total pressure, lb/sq ft

p static pressure, lb/sq ft

R height of duct at measuring stations, ft

r distance measured from duct floor, ft

S   distance between the end of the primary nozzle and the end of the external shroud, ft

$\dfrac{S}{D_p}$ ejector spacing ratio

T   total temperature, $^\circ$R

V   velocity, ft/sec

$\dfrac{W_s\sqrt{T_s}}{W_p\sqrt{T_p}}$ ejector weight-flow ratio

x   axial distance, in.

y   distance from the model surface to a point in the boundary layer, in.

α external cowl angle, deg

β inlet floor angle of turn, deg

γ ratio of specific heats

δ boundary-layer thickness, in.

θ wrap around angle of rectangular scoop inlets, deg

φ circumferential location (0 on top of model), deg

Subscripts:

b   boundary layer

c   conditions of inlet cowl lip

D   drag

l local

p   primary

s   secondary

x   axial station

0   free stream

1   cowl lip

2   inlet discharge

3   nozzle

APPARATUS AND PROCEDURE

The model installed in the Lewis 8- by 6-foot supersonic wind tunnel is shown in figure 1, and internal model details are given in figure 2. The secondary air flow captured by the auxiliary inlets was ducted back past the total-pressure rake at the inlet-discharge station, through a divergent fairing, and dumped into the annular secondary passage. The primary air, which was obtained from the service-air facilities of the laboratory, was preheated to 250° F and then passed through the hollow support struts into the model. Details of the basic model and its tunnel installation are given in reference 5.

Eight normal-shock auxiliary inlets were investigated, some in conjunction with both of the two ejectors studied and the others with only one of the two ejectors. Details of the various inlets are shown in figure 3. The submerged inlet (fig. 3(a)) had a 7° ramp and a sharp lip flush with the model surface. The scoop height of the series of four rectangular scoop inlets (fig. 3(b)) tested varied from 0.239 to 0.653 inch, while the wrap around angle was held fixed. A pair of rectangular scoop inlets each of one half the aspect ratio and approximately the same height as rectangular inlet 0.324 were also investigated. These dual inlets were mounted diametrically opposed ($\varphi = 0°$ and $180°$) with the top inlet in the same position ($\varphi = 0°$) as the single rectangular inlets investigated. A diverter plate was installed on rectangular inlet 0.653 to plow off the lower energy boundary layer. This configuration is designated as inlet 0.653-S (fig. 3(c)). All the rectangular inlets had sharp-lipped cowls with an included lip angle of 8°. A number of the inlets were instrumented with static orifices in order to measure external pressure drag. A pair of circular inlets mounted in the same position as the dual rectangular inlets ($\varphi = 0°$ and $180°$) was also investigated (fig. 3(d)). The cowl lips were sharp and symmetrical in crosssection with a 16° included angle.

The details of the two ejectors investigated are shown in figure 4. Figure 4(a) shows the details of the ejector having a diameter ratio of 1.158 and a spacing ratio of 0.800. This ejector will be referred to as ejector 1.16-0.80. In figure 4(b), the details of the ejector with a 1.304 diameter ratio and 0.808 spacing ratio are shown. Similarily, this ejector will be referred to as ejector 1.30-0.80.

3809

The flow area variations from station 1 to the discharge stations of the eight auxiliary inlets investigated are shown in figure 5(a). The area variation of the secondary flow passage, from the inlet-discharge station to the nozzle station, is shown in figure 5(b). The abrupt increase in secondary flow passage area results from the dumping of the inlet air flow into the annular secondary passage at the end of the faired discharge (fig. 2).

The flow conditions ahead of the inlet were investigated in order to determine the boundary-layer profile and thickness. Usual total- and static-pressure instrumentation were employed. As shown in figure 6, the boundary layer had very nearly a one-seventh power profile.

Prior to the investigation of the over-all inlet-ejector systems, the ejectors were individually evaluated, as in reference 5, in order to determine their pumping characteristics. The primary and secondary air were obtained from the same source and a sliding bleed valve was used to throttle the secondary flow. The primary total pressure and weight flow were calculated from static pressures at the primary nozzle entrance and from a prior calibration of the primary nozzle. The secondary weight flow was obtained from a calibrated throttling valve (ref. 5). Secondary total-pressure ratio was measured with rakes mounted at the nozzle station as shown in figure 4.

When the auxiliary inlets were installed, the inlet mass flow was obtained from the known ejector pumping characteristics and the secondary nozzle-station total pressure. Total-pressure recoveries were measured at both the inlet-discharge station and at the end of the secondary-flow passage (nozzle station). The total-pressure rake at the inlet-discharge station had forward and rearward facing tubes (fig. 2). These total pressures along with the secondary total temperature (measured by the thermocouples shown in fig. 4(a)) were used to determine the direction of the flow in the secondary passage. Total pressures at the inlet discharge and nozzle stations were averaged on an area weighted basis.

RESULTS AND DISCUSSION

Inlet performance. - Pressure-recovery mass-flow characteristics at zero angle of attack are presented in figure 7 for the auxiliary inlets investigated. The pressure recovery is at the inlet-discharge station, prior to the dumping of the flow into the full annulus. Inlet mass flow was obtained from pressure data and the previously obtained ejector pumping characteristics. In some cases the subcritical portion of the inlet maps have been extrapolated to an estimated value of pressure recovery at zero mass flow. These values were obtained from the ejector pumping characteristics and the reverse flow limit discussed later in this report.

Although the pressure recovery of the submerged inlet (fig. 7(a)) appears low, the results are comparable with those reported in reference 1. The rectangular scoop having the lowest height (inlet 0.239 with a scoop height to boundary-layer thickness ratio $\frac{h}{\delta}$ of 0.195 at free-stream Mach number M_0 of 2.0) indicated higher pressure recovery than the submerged. Further gains resulted as the scoop inlet height was increased. However, this was accompained by a continuing sharper pressure-recovery decrease as the inlet was operated subcritically.

The effect of inlet aspect ratio is apparent from a comparison of inlets 0.324 (fig. 7(d)) and 0.345-D (fig. 7(e)). Inlet 0.345-D had about the same capture area and scoop height as inlet 0.324 but consisted of two inlets on opposite sides of the body ($\varphi = 0^\circ$ and 180°) each having about 1/2 the aspect ratio of inlet 0.324. A reduction in the critical mass-flow ratio and pressure recovery resulted from a decrease in the aspect ratio. The subcritical pressure-recovery characteristics were also altered.

Application of the splitter-plate technique commonly used on body-mounted main inlets was attempted on one of the boundary-layer auxiliary inlets. The splitter plate effect may be noted from a comparison of the original inlet 0.653 (fig. 7(f)) and the revised 0.653-S inlet with splitter plate (fig. 7(g)). Apparently the splitter plate did not divert the lower energy air since its effect was to reduce slightly the critical mass-flow ratio and not to generally affect the peak-pressure recovery. Based on the limited data available, the splitter reduced the amount of pressure-recovery decrease when the inlet was operated subcritically.

The large increase in the peak-pressure recovery with the use of the circular inlets (fig. 7(h)) is largely due to the higher energy air captured by these inlets. For example, at a Mach number of 2.0, about 35 percent of the captured air flow was from outside the boundary layer. In reference 2, numerous idealized circular-inlet configurations were tested while mounted on a flat plate and without internal duct bends. Because the circular inlets reported herein were not of exactly the same boundary-layer position as reported in reference 2, no direct comparison between the idealized and more practical inlets is possible. However, these results (fig. 7(h)) were about 5 to 10 percent below that which would be estimated from the data of reference 2. This difference probably was due to higher subsonic losses encountered herein.

Flow instability (pulsing) was noted when the 0.512 and 0.653 rectangular inlets were operated under subcritical conditions. In general, an increase in scoop height of the rectangular inlets increased this tendency to be unstable subcritically. It should be noted that, although not apparent from figure 7(g), use of the splitter (inlet 0.653-S) resulted in spasmodic instability over the entire mass-flow range. No tendency to pulse was noted for the circular inlets.

The maximum theoretical mass-flow ratios that the scoop inlets may capture from the boundary layer (obtained from ref. 4) are indicated in figure 7. Except for inlets 0.345-D and 0.653-S, the supercritical mass flow ratios were generally close to the theoretical maximum. Similar agreement was noted for the circular inlets reported in reference 2.

The performance of the inlets under angle of attack operation at a Mach number of 2.0 are shown in figure 8. For the single inlet configurations ($\varphi = 0^{\circ}$) positive angles of attack resulted in lower pressure recovery whereas negative angles resulted in increases in pressure recovery. These results are as would be expected since positive angle of attack thickened the boundary layer ahead of the inlets, whereas negative angles thinned the boundary layer. The use of dual inlets reduced the angle of attack effect as might be expected.

The pressure recovery data of figure 7 has been cross-plotted to show the effect of the ratio of inlet height to boundary-layer thickness $\frac{h}{\delta}$ and is presented in figure 9. The theoretical pressure recovery possible for an inlet in a boundary layer having a one-seventh power profile without internal losses is included. Although the pressure recovery increased with h/δ at about the same rate as theoretical, the experimental results were approximately 68 to 75 percent of the theoretical values. These large internal losses may have resulted from the rapid turn (25°) of the duct floor near the cowl-lip station and the relatively sharp turn of the duct roof just ahead of the rake.

The total-pressure profiles at the inlet-discharge station varied from inlet to inlet. In figure 10 is shown the effect of scoop height on these profiles for critical inlet operation. The total-pressure peak shifted toward the center of the duct and the distortions became more severe as the scoop height was increased. Because the velocity difference across the entering boundary-layer flow is greater as h/δ is increased it might be expected that profiles at the inlet-discharge station would become more severe.

The effect of the inlet operating conditions on the total-pressure profiles at the inlet discharge is shown for rectangular inlet 0.324 (fig. 11). The distortion was small during subcritical operation but increased in severity as critical operation was approached. Supercritical operation resulted in the most severe distortion.

Static-pressure orifices were installed on the external cowl of several inlets in order to obtain pressure drag. A sample of the pressure distributions observed is shown in figure 12. Integration of these pressures yielded the inlet pressure drags presented in figure 13. For all configurations instrumented, the inlet pressure drag increased as the mass-flow ratio was decreased. This increase in cowl pressure drag is

opposite to that generally noted with nose inlets because primarily the exterior slope of the auxiliary inlets was opposite to that of main inlets. When the inlet was supercritical, the external drag of inlet 0.653-S (not including the force on the diverter) was a function of the internal shock position. This effect, which is not the apparent scatter in figure 13, may have been caused by pressure feedback influencing the shock formation about the diverter which in turn influenced the pressures on the inlet cowl.

Performance of secondary-flow passage. - When the air delivered by an auxiliary inlet is to be used in an ejector, the flow must be distributed into the annular secondary passage. The section of duct between the inlet-discharge station and the primary-nozzle station has been termed the secondary-flow passage. In the present investigation, the secondary passage (fig. 5) consisted of a rapid area change with the use of the fairings as shown in figure 2 and of the dumping from the inlet into the full annular duct, which provided passage for the air back to the nozzle station. The total-pressure loss associated with this type of passage is shown in figure 14. Data were included for all configurations and free-stream Mach number. Apparently the loss in total pressure was primarily a function of the secondary-passage inlet Mach number. The greater part of this loss probably resulted from the dumping of the flow rapidly into an area that was nine times the size of the entering flow. The total-pressure loss was proportional to the square of the inlet-discharge Mach number.

The auxiliary-inlet total-pressure recovery that is available to an ejector does, of course, include the losses encountered in the secondary-flow passage. Thus, the effective inlet pressure recovery is a function of the Mach number at the inlet-discharge station, which depends upon the inlet capture area. Consequently, the smaller inlets tested only encountered small losses in critical pressure recovery; whereas, the larger inlets encountered higher losses. If, in the design of an inlet-ejector system, these losses in the secondary duct are considered too great, they can be reduced by a more gradual area change from the inlet discharge to the full annular passage.

Total-pressure profiles at the nozzle station are presented in figure 15(a) in order to show the circumferential distribution of the flow in the annular secondary-flow passage. The profiles were taken at half the duct height and for the inlets operating near critical. For the single inlet configurations, the nonuniformity in the circumferential flow distribution was reduced as the scoop height was decreased. This flow distortion was not symmetrical about the vertical center line although the inlets and the passage were. As might be expected, the use of dual inlets 180° apart minimized the circumferential flow distortions (compare inlets 0.324 and 0.345-D). If a single circular inlet had been investigated, a profile more severe than that shown for the dual circular inlets might be expected. Apparently, the circumferential flow distribution may be poorest for single auxiliary inlets with high performance.

3809

Radial profiles were measured at the nozzle station for all configurations. Typical of these profiles are those for inlet 0.653 (fig. 15(b)). The largest distortion was generally on the top of the duct directly downstream of the inlet discharge ($\varphi = 0^\circ$) and was similar in shape to that noted at the inlet-discharge station. The inlet operating condition apparently influenced the radial profiles at the two stations in about the same way.

Inlet operation influenced the circumferential flow distribution at half the duct height in the manner shown in figure 15(c) for inlet 0.653. Again the poorest profiles were obtained with supercritical operation of the inlet. Although the ejector weight-flow ratio $\dfrac{W_s\sqrt{T_s}}{W_p\sqrt{T_p}}$ varied under supercritical inlet operation, the secondary flow was constant $(m_s/m_0 = \text{constant})$.

CM-2

Ejector pumping characteristics. - The two ejectors used in conjunction with the auxiliary inlets were investigated separately over a wide range of pressures and weight-flow ratios. These tests were made with a bleed valve between the primary and secondary flows (ref. 5). The ejectors are designated by their diameter ratio $\dfrac{D_s}{D_p}$ and spacing ratio $\dfrac{S}{D_p}$, respectively. Pumping characteristics for ejectors 1.16-0.80 and 1.30-0.80 are presented in figure 16. External Mach number at the low pressure ratios appears to have the same effect as reported in reference 6. When the secondary flow was unchoked, the low base pressure became apparent in the secondary system and lowered the secondary pressure required to pass a given weight flow.

Conversion of the experimental ejector pumping characteristics (fig. 16) from P_3/P_p to P_3/P_0 has been made and the results are shown in figure 17. The inlet pressure recovery required for the ejector to handle a certain weight flow at a given primary-nozzle pressure ratio are indicated directly. The relatively low slope of these curves emphasizes the large effect of inlet-pressure recovery on ejector weight-flow ratio.

Auxiliary inlet-ejector configuration performance. - The following equation (developed in ref. 4) relates the operation of the combined system of primary nozzle, secondary air flow, and the auxiliary inlet:

$$\frac{W_s\sqrt{T_s}}{W_p\sqrt{T_p}} = \frac{m_s}{m_0}\frac{A_c}{A_p}\sqrt{\frac{T_s}{T_0}}\frac{K_1}{P_p/P_0} \tag{1}$$

where

$$K_1 = M_0\left(1 + \frac{\gamma_0 - 1}{2} M_0^2\right)^{1/2} \left(\frac{\gamma_p + 1}{2}\right)^{\frac{\gamma_p+1}{2(\gamma_p-1)}} \sqrt{\frac{\gamma_0}{\gamma_p}} \qquad (2)$$

If the inlet map and ejector map were converted to the same weight-flow parameter by equation (1), at any free-stream Mach number the primary nozzle pressure ratio P_p/p_0 determines the operating condition of a fixed inlet $\left(\frac{A_c}{A_p} \text{ fixed}\right)$ and also the ejector weight-flow ratio $\frac{W_s\sqrt{T_s}}{W_p\sqrt{T_p}}$.

Conversely, a desired weight-flow ratio may be obtained by selecting the proper inlet size at the known free-stream Mach number and P_p/p_0. The inlet pressure recovery necessary for the ejector to handle the desired weight-flow ratio may be obtained from ejector curves such as figure 17, and the inlet mass-flow ratio may be obtained from the inlet map. The required inlet size may then be computed from equation (1).

Each configuration tested in this investigation consisted of a fixed inlet and fixed primary nozzle ejector. Consequently, A_c/A_p was fixed for each inlet-ejector configuration. At each test Mach number the primary pressure ratio was varied. This in turn determined all of the inlet and ejector conditions.

The effect of primary nozzle operation on pressure recovery delivered by the various inlets is shown in figure 18. At low primary pressure ratios, the inlets were operating supercritical. As the pressure ratio was increased the inlets approached critical and the pressure recovery increased. Further increases in primary pressure caused subcritical operation with either increasing or decreasing pressure recovery, depending on the inlet. Eventually, the primary pressure ratio was sufficiently high to stop the inlet flow altogether. This has been termed the reverse flow limit since further primary pressure ratio increases resulted in the flow from the primary jet being exhausted through the inlet.

If, at a given primary nozzle pressure ratio, the pressure recovery delivered by the inlet is less than the pressure recovery required by the ejector for zero secondary flow, reverse flow will result (ref. 4). The limiting curve, therefore, is the relation of pressure-recovery to primary-pressure ratio for zero secondary weight flow as obtained from the ejector pumping maps (fig. 17). The results shown in figure 18 indicate good agreement between the experimental and predicted reverse-flow limits.

Reverse flow could be measured from either total-pressure measurements (fig. 2) at the inlet-discharge station or total-temperature measurements in the secondary flow passage (fig. 4). Typical data (inlet 0.239, ejector 1.16-0.80) are shown in figure 19. An increase in secondary temperature is obtained as reverse flow is approached because of the reduced secondary (coolant) air flow. When this flow was zero, the secondary temperature essentially reaches its maximum value, which for all conditions was about 93 to 94 percent of the primary jet temperature. The ratio of the forward to rearward facing total pressures at the inlet-discharge station indicates a value greater than unity for positive flow and less than unity for negative flow. Of the two methods employed to determine reverse flow, the temperatures yielded the more consistent results.

The effect of primary-pressure ratio on the ejector weight-flow ratio obtained with the fixed inlet-ejector combinations are presented in figure 20. Three inlets are shown for each ejector. Each inlet had a different type of inlet-pressure-recovery characteristics as shown in figure 21. The variation of the curves under supercritical inlet flow agrees with equation (1), which indicates that $\dfrac{W_s\sqrt{T_s}}{W_p\sqrt{T_p}} \times \dfrac{P_p}{P_0} = \text{constant}$ if the inlet is supercritical. When the inlets were operated subcritically, the variation of $\dfrac{W_s\sqrt{T_s}}{W_p\sqrt{T_p}}$ was dependent on the inlet pressure-recovery mass-flow characteristics.

In order to properly design an auxiliary boundary-layer inlet which supplies secondary air flow to a known ejector, the type of inlet must represent a compromise between low inlet-air momentum (low h/δ) and high pressure recovery (high h/δ). This problem is more completely discussed in reference 4. Once the type of inlet and location (h/δ) have been chosen, the capture area of the inlet may be obtained from equation (1) and the inlet and ejector maps. The number of inlets used and the inlet aspect ratio can than be computed.

The effect of inlet size on the ejector weight-flow ratio is shown in figure 22. An inlet having the performance of inlet 0.653 (fig. 16(d)) and an ejector having the pumping characteristics of ejector 1.30-0.80 (fig. 22) were assumed. Curves for various primary-nozzle pressure ratios are shown, and operation with the inlet at critical is also indicated.

The family of straight lines describe supercritical inlet operation because $\dfrac{W_s\sqrt{T_s}}{W_p\sqrt{T_p}}$ is a direct function of A_c/A_p. The $\dfrac{W_s\sqrt{T_s}}{W_p\sqrt{T_p}}$ at critical inlet operation is established by the critical inlet pressure

recovery, (figs. 17(b) and 21). Since the pressure recovery of the inlet considered decreases subcritically, the weight-flow ratio also decreases as the inlet size is increased at a given primary pressure ratio. If the inlet had performance such as obtained with the circular inlets, the weight-flow ratio would increase under subcritical inlet operation as the pressure recovery increased.

The effect of primary-nozzle pressure ratio with a given-size inlet on weight-flow ratio is also apparent from figure 22. As the pressure ratio is increased, the weight-flow ratio is decreased. At a pressure ratio of 9.3 the pressure recovery required by this ejector is the same as the auxiliary-inlet pressure recovery at zero flow. Consequently, the inlet and ejector will match at zero secondary flow. However, (as shown in fig. 22) operation with positive flow is also possible at this pressure ratio. The reason for these two match points can readily be seen from figure 23(a) where the inlet and ejector maps are superimposed. Two match points result because the subcritical inlet pressure recovery had a greater slope than the ejector pumping characteristics. Two match points are also possible at primary pressure ratios greater than 9.3. At a ratio of 10, for example, two operating points would result (figs. 22 and 23(b)) if A_c/A_p is less than 0.08. The inlet and ejector curves would not intersect at a P_p/P_0 of 10.0 if A_c/A_p was greater than 0.08. Reverse flow would result for all inlet sizes at primary pressure ratios greater than 11.0 since the maximum pressure recovery the inlet could deliver would then be less than the minimum pressure recovery the ejector would tolerate $\left(\text{at } \dfrac{W_s\sqrt{T_s}}{W_p\sqrt{T_p}} = 0 \right)$.

SUMMARY OF RESULTS

The following results were obtained from an investigation of auxiliary-inlets supplying secondary air flow to ejector exhaust nozzles. The tests were conducted over a wide pressure-ratio range at free-stream Mach numbers of 0.64, 1.5, 1.8, and 2.0.

1. Auxiliary-inlet pressure recovery increased with scoop height at about the same rate as theoretically predicted for an inlet in a boundary layer having a one-seventh power profile. However, the experimental values of pressure recovery were approximately 68 to 75 percent of the theoretical, indicating large internal losses.

2. An increase in scoop height of the rectangular-scoop inlets increased their tendency to pulse during subcritical operation.

3. Uneven circumferential flow distribution at the secondary air-flow entrance of the ejector was noted with single inlets having high pressure recovery. The use of two inlets 180° apart in place of one resulted in a better distribution of the flow.

4. Flow from the primary jet was exhausted through the auxiliary inlet under some operating conditions which could be predicted from the ejector pumping characteristics.

5. If the relative slope of the subcritical portion of the inlet pressure recovery map is greater than that of the ejector pressure recovery requirement curve, two match points, each with a different weight flow, may be possible.

Lewis Flight Propulsion Laboratory
    National Advisory Committee for Aeronautics
        Cleveland, Ohio, October 17, 1955

REFERENCES

1. Pennington, Donald B., and Simon, Paul C.: Internal Performance at Mach Numbers to 2.0 of Two Auxiliary Inlets Immersed in Fuselage Boundary Layer. NACA RM E53L28b, 1954.

2. Simon, Paul C.: Internal Performance of a Series of Circular Auxiliary-Air Inlets Immersed in a Turbulent Boundary Layer Mach Number Range: 1.5 to 2.0. NACA RM E54L03, 1955.

3. Goelzer, H. Fred, and Cortright, Edgar M., Jr.: Investigation at Mach Number 1.88 of Half of a Conical-Spike Diffuser Mounted as a Side Inlet with Boundary-Layer Control. NACA RM E51G06, 1951.

4. Hearth, Donald P., Englert, Gerald W., and Kowalski, Kenneth L.: Matching of Auxiliary Inlets to Secondary-Air Requirements of Aircraft Ejector Exhaust Nozzles. NACA RM E55D21, 1955.

5. Hearth, Donald P., and Valerino, Alfred S.: Thrust and Pumping Characteristics of a Series of Ejector-Type Exhaust Nozzles at Subsonic and Supersonic Flight Speeds. NACA RM E54H19, 1954.

6. Stitt, Leonard E., and Valerino, Alfred S.: Effect of Free-Stream Mach Number on Gross-Force and Pumping Characteristics of Several Ejectors. NACA RM E54K23a, 1955.

Closeup of inlet
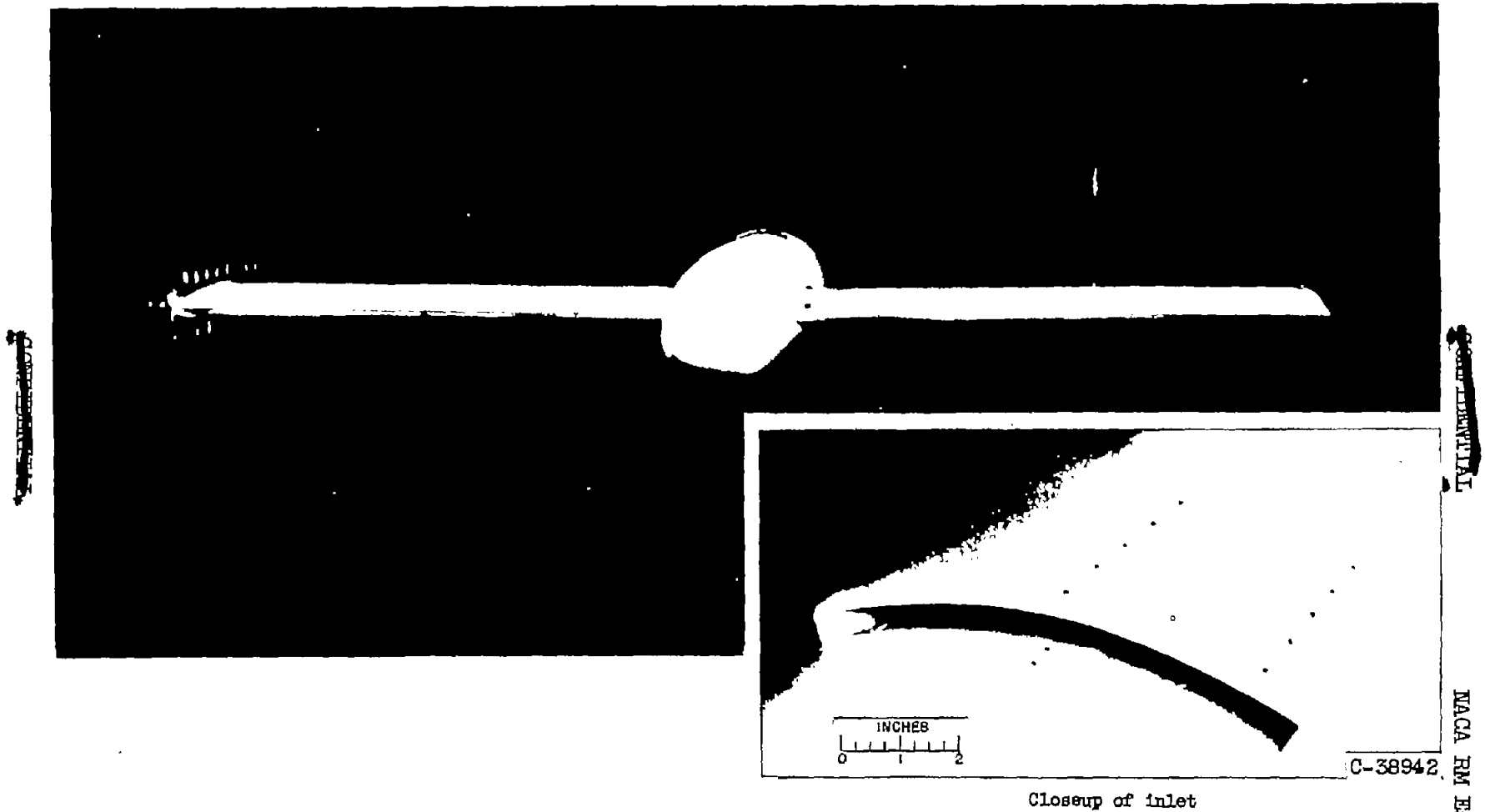
Figure 1. - Model in Lewis 8- by 6-foot supersonic wind tunnel.

Hollow support struts — Inlet

Nozzle,
station 3

Honeycomb

Model
stations 0

Parabolic nose section

Cylindrical
section

40.00

50.75
Inlet cowl starts

74.66

Cowl lip,
station 1

Inlet discharge,
station 2 — Total-pressure rake

Fairings

Honeycomb
primary jet

CD-4262

Figure 2. - Jet-exit model.

3809

Section A-A

Section B-B

(a) Submerged inlet.

Lip station
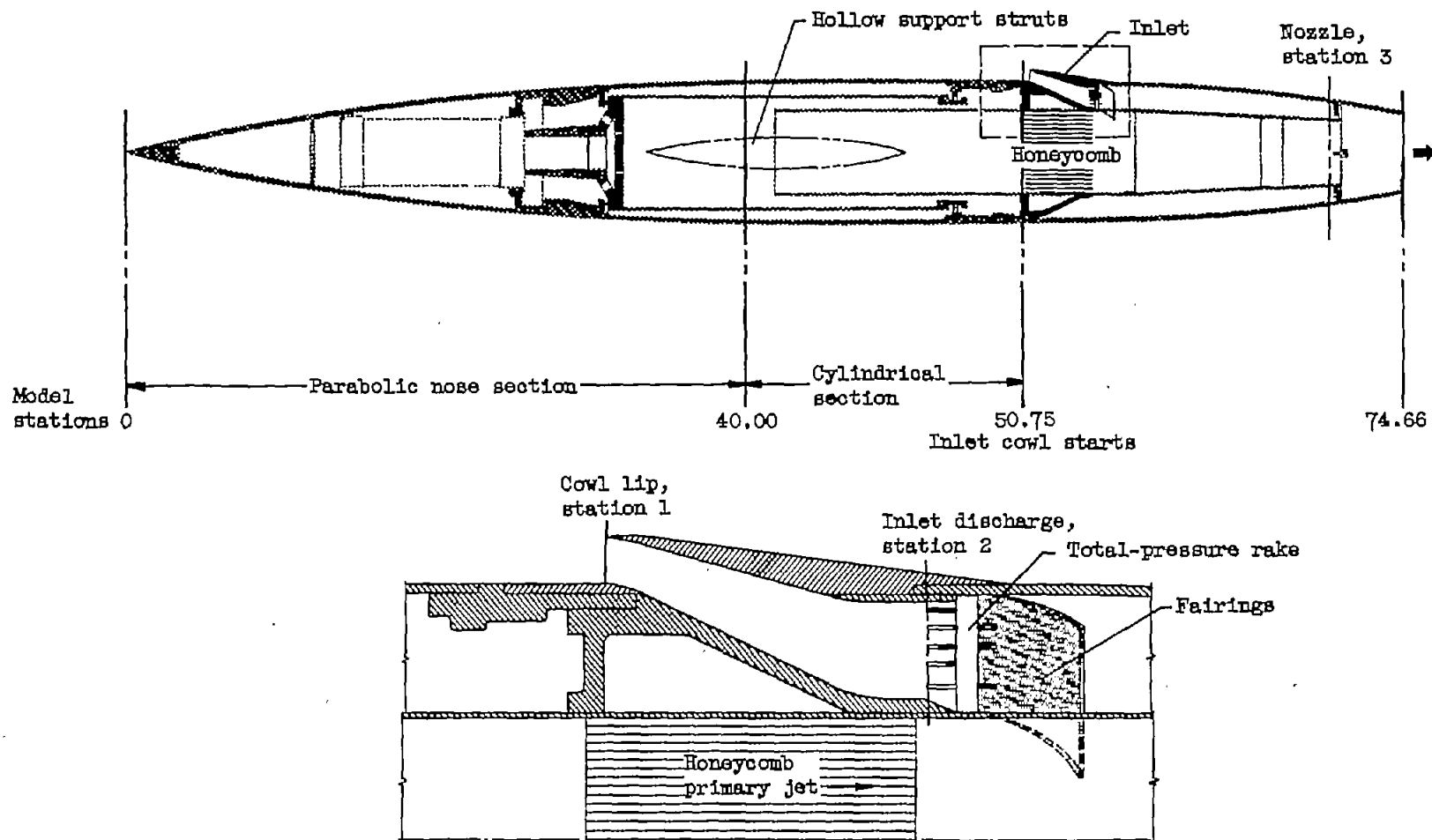
Station 2
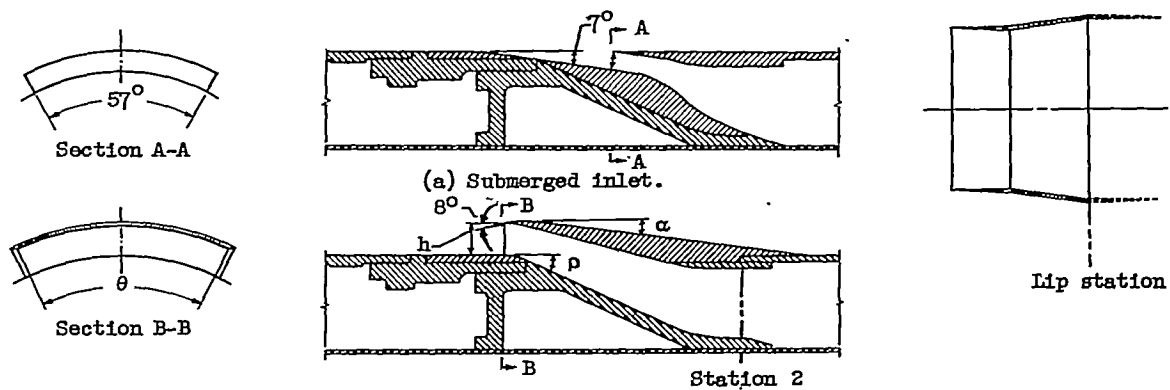
Inlet	Inlet height h in.	External cowl angle α deg	Inlet floor angle of turn β deg	Wrap around angle θ deg
0.239	0.239	$6\frac{1}{2}$	25	51
.324	.324	$7\frac{1}{2}$	25	51
.512	.512	$6\frac{1}{2}$	25	51
.653	.653	$6\frac{1}{2}$	25	51
.345-D	.345	$7\frac{1}{2}$	25	$2 @ 25\frac{1}{2}$

(b) Scoop inlet.

Section C-C

0.653   0.505   0.150

(c) Inlet 0.653-S.

Section D-D

CD-4534
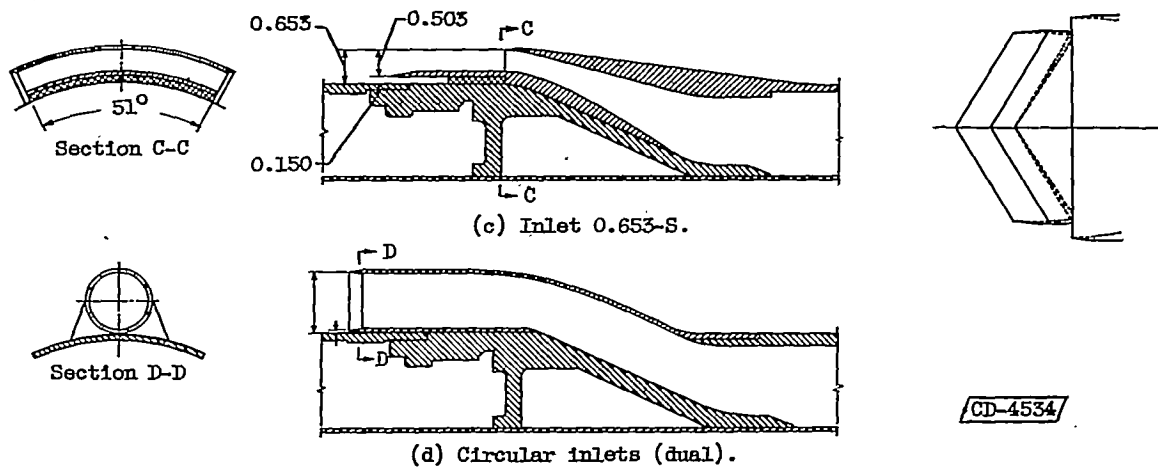
(d) Circular inlets (dual).

Figure 3. - Details of inlets.

3809

CM-3
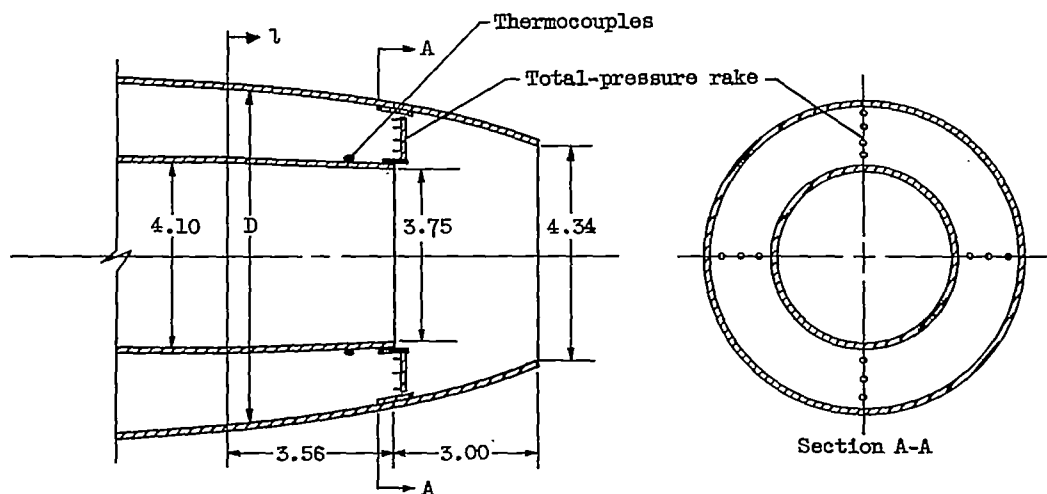
(a) Ejector 1.16-0.80; ejector diameter ratio, 1.158; ejector spacing ratio, 0.800.
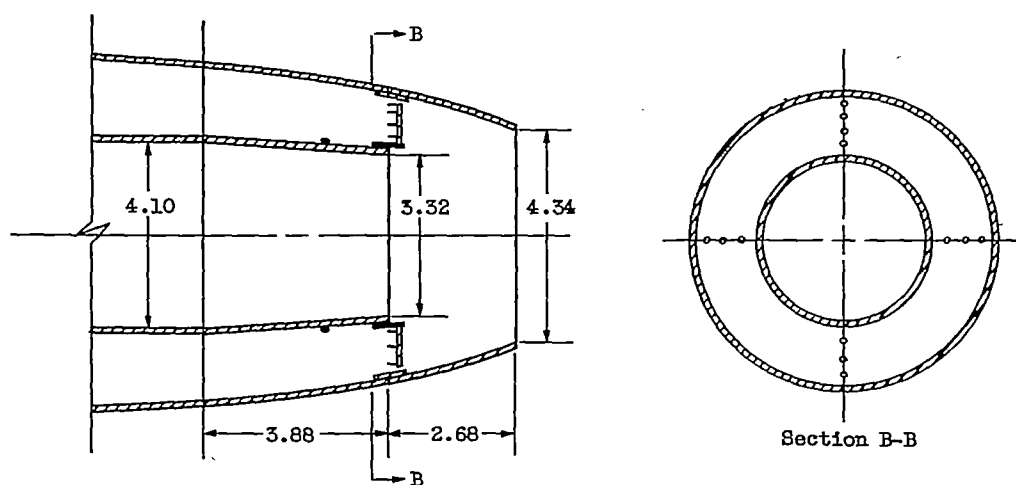
Axial station ł, in.	3.56	3.88	4.33	5.00	5.50	6.00	6.56
Inside diameter D, in.	5.60	5.50	5.80	5.43	5.17	4.84	4.34

Coordinates of outer shroud

(b) Ejector 1.30-0.80; ejector diameter ratio, 1.304; ejector spacing ratio, 0.808.

Figure 4. - Details of ejectors. (All dimensions in inches.) /CD-4535/
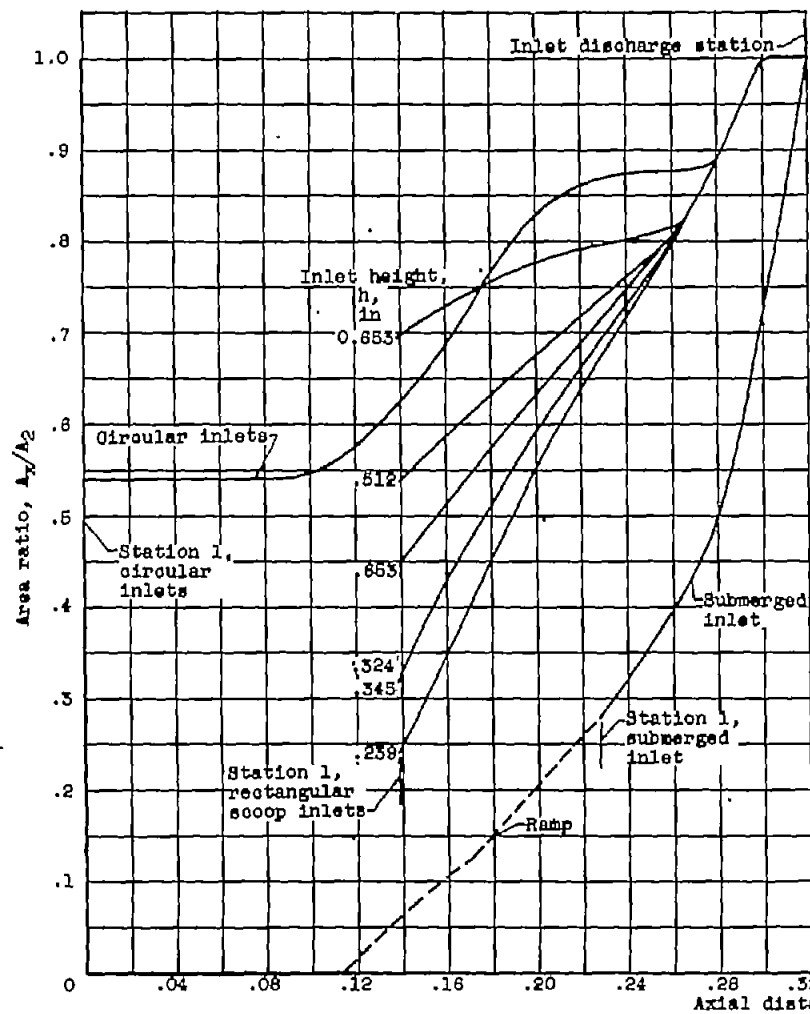
(a) Area variation from station 1 to inlet discharge station;
inlet-discharge area for all scoop inlets, 0.02588 square
feet; inlet-discharge area for submerged inlet, 0.0289
square feet.
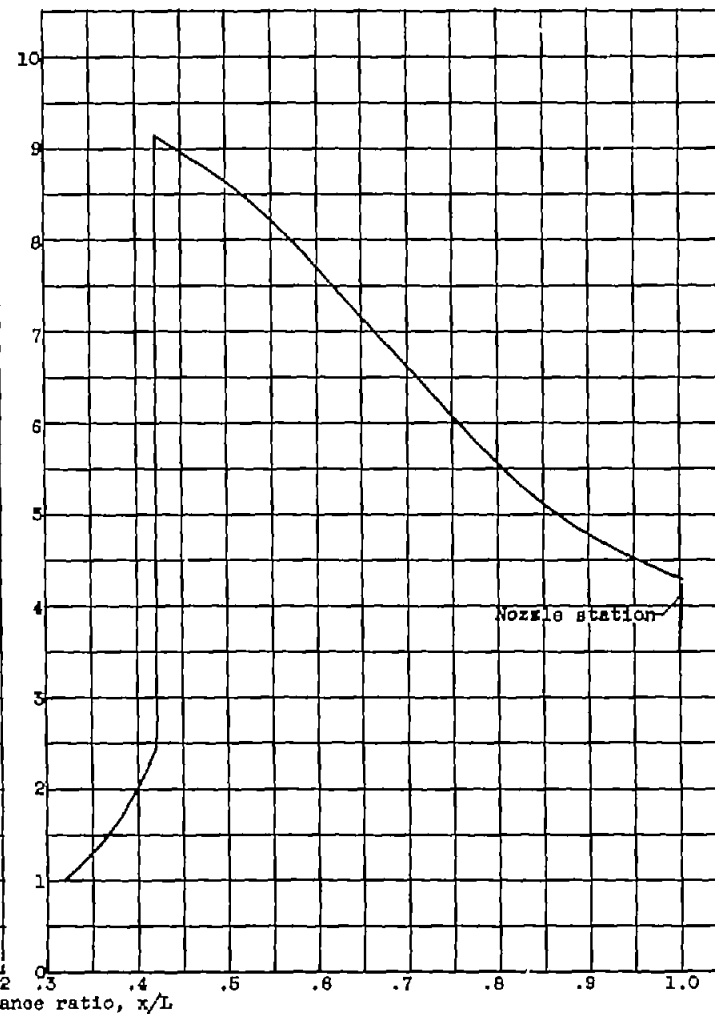
(b) Area variation from inlet-discharge station to nozzle
station; inlet-discharge area, 0.02588 square feet.

Figure 5. - Flow area variation; total length, 2.029 feet.
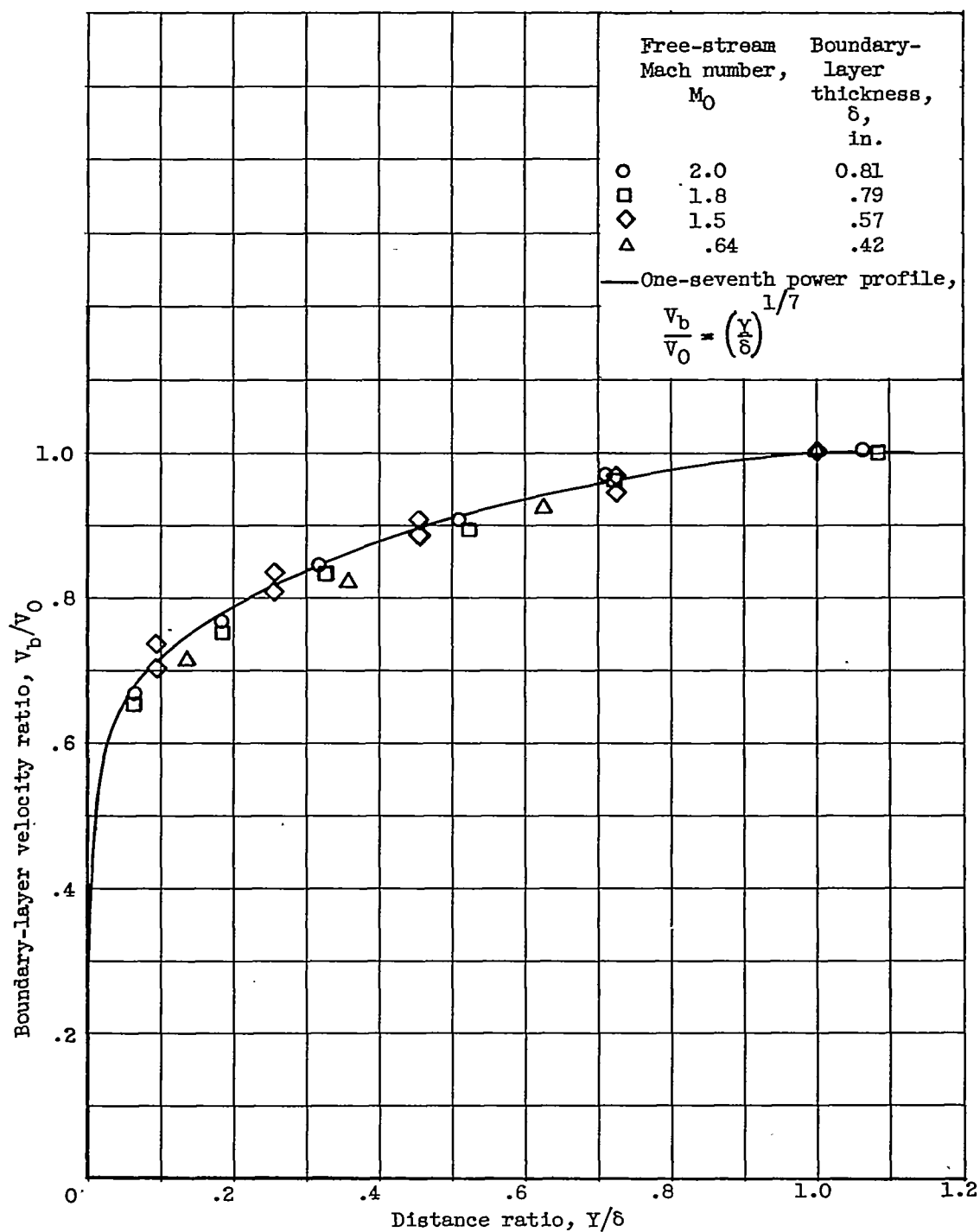
Figure 6. - Boundary-layer profile ahead of inlet at zero angle of attack.

(a) Submerged inlet.

(b) Inlet 0.239.

(c) Inlet 0.512.
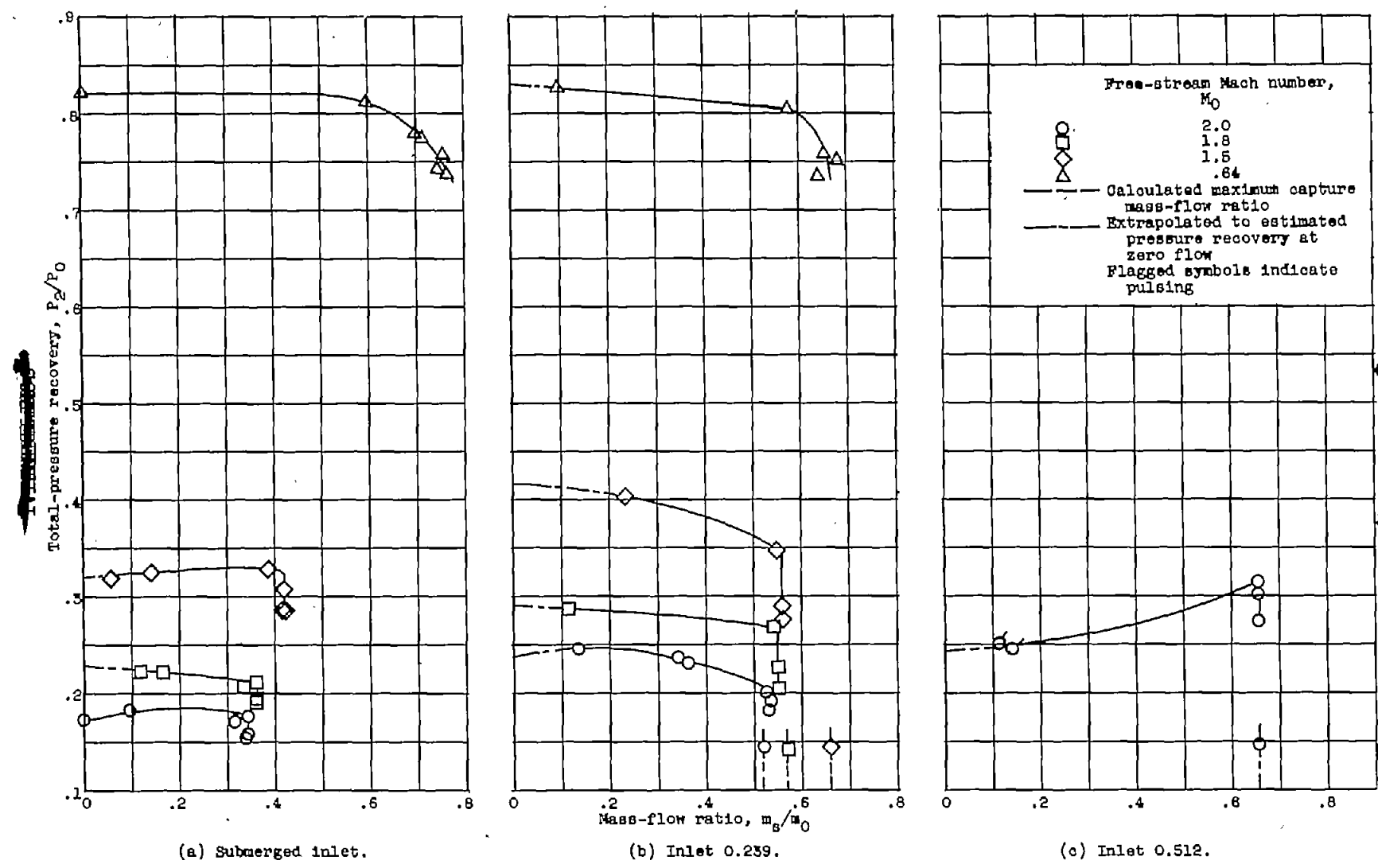
Figure 7. - Inlet performance characteristics at zero angle of attack.
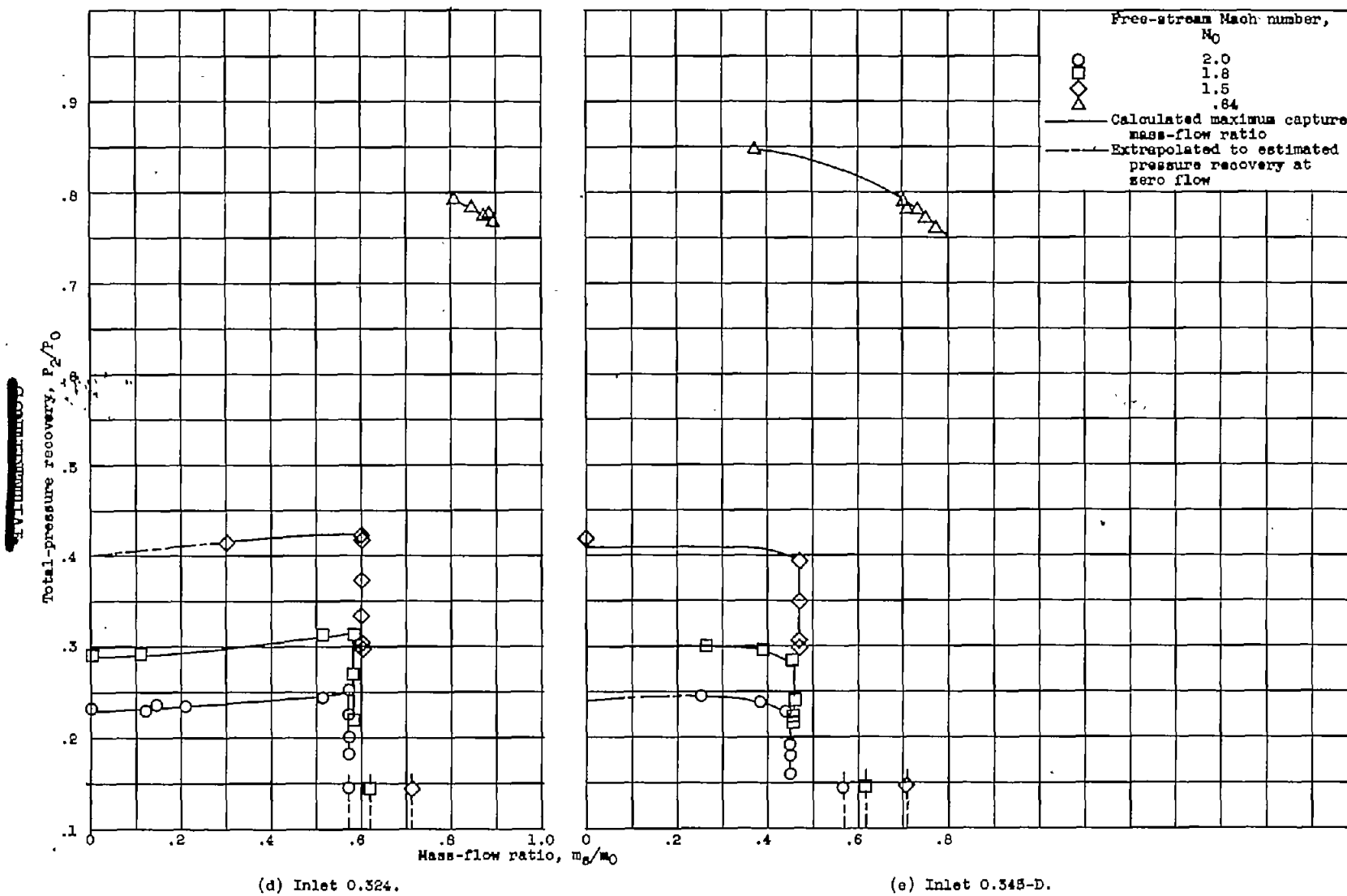
(d) Inlet 0.324.

(e) Inlet 0.345-D.

Figure 7. - Continued. Inlet performance characteristics at zero angle of attack.

(f) Inlet 0.653.

(g) Inlet 0.653-S.

Figure 7. - Continued. Inlet performance characteristics at zero angle of attack.

3809
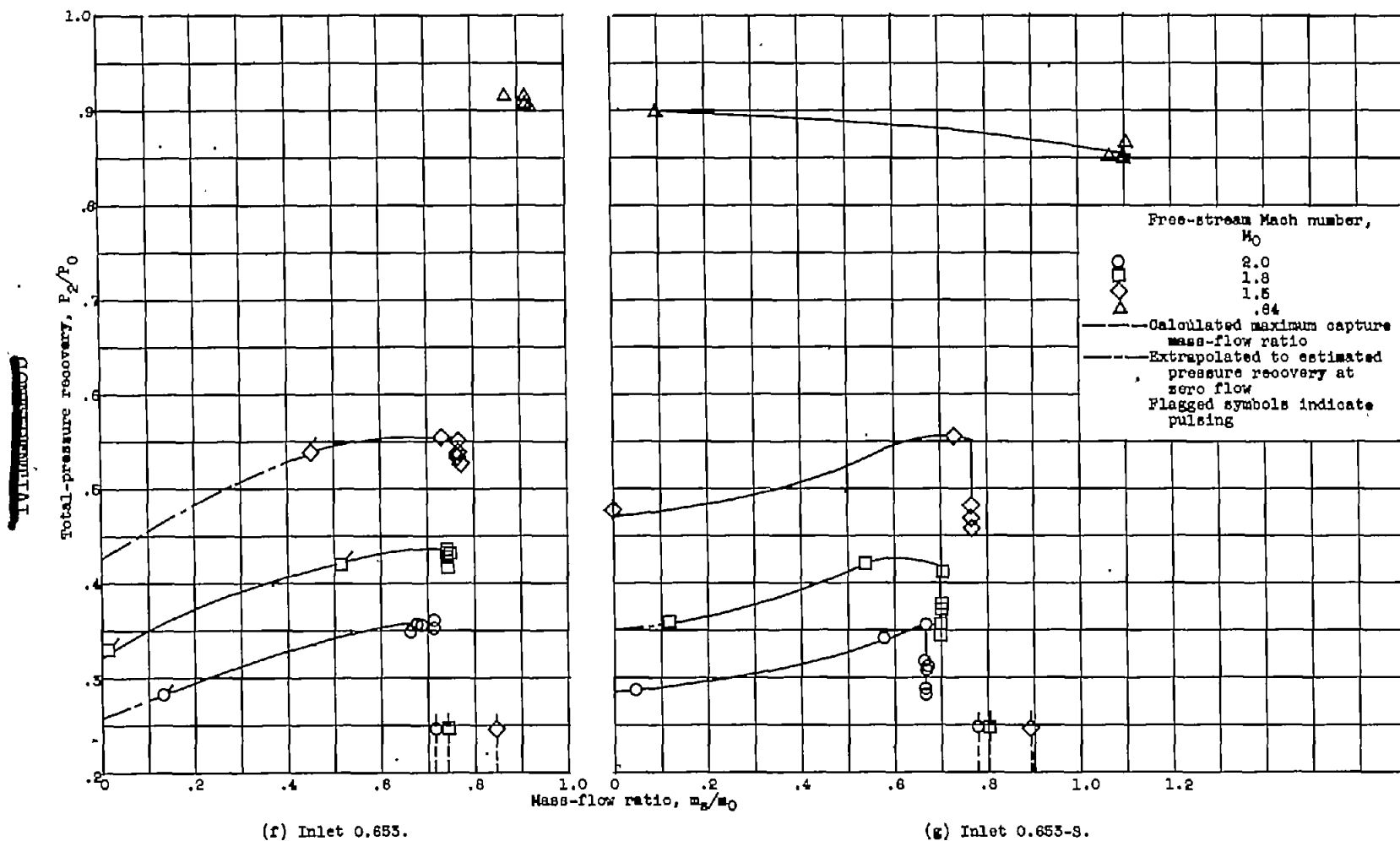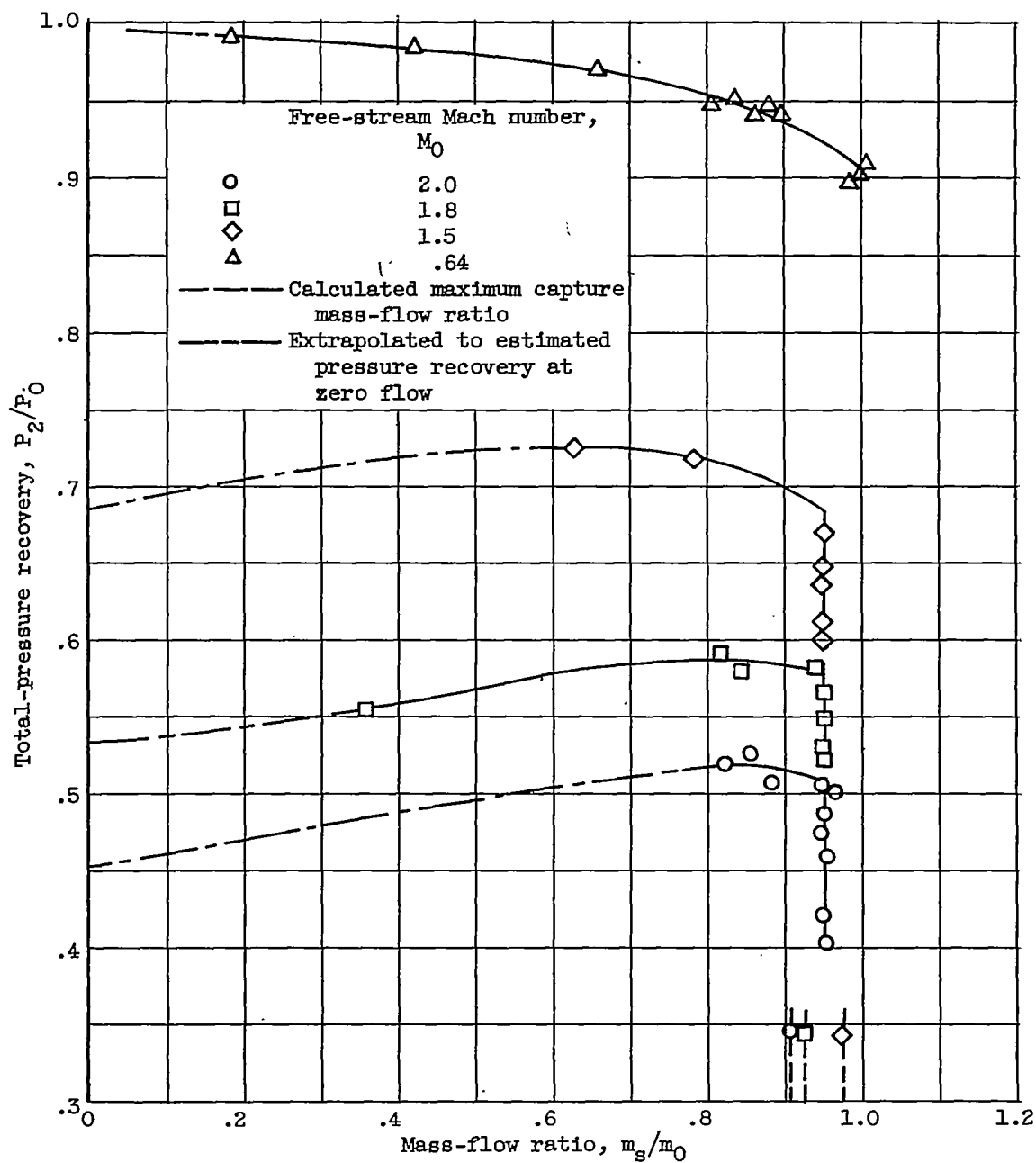
(h) Circular inlets.

Figure 7. - Concluded. Inlet performance characteristics at zero angle of attack.

(a) Submerged inlet.

(b) Circular inlets.

(c) Inlet 0.653.

(d) Inlet 0.653-S.
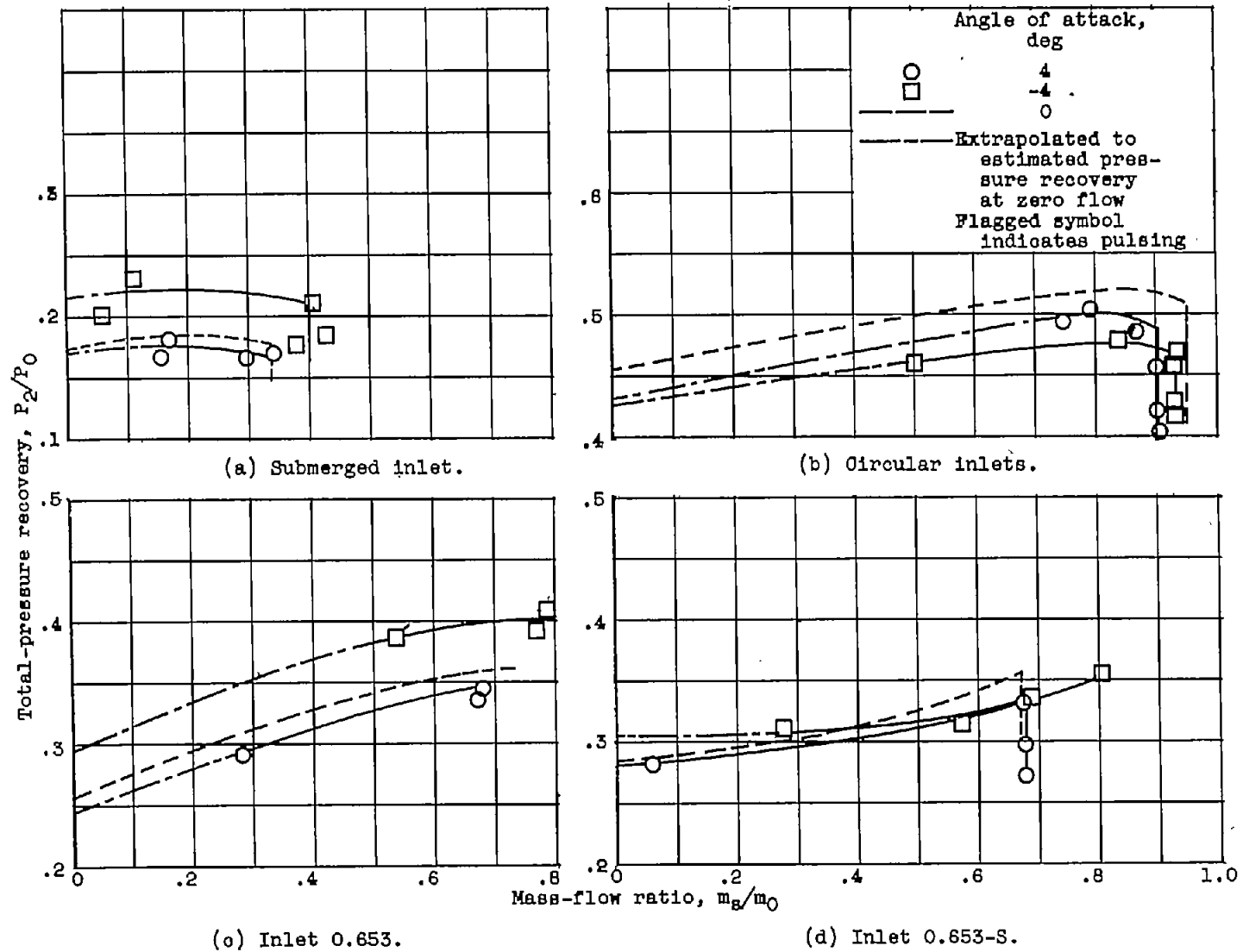
Figure 8. - Effect of angle of attack on inlet performance characteristics; free-stream Mach number, 2.0.

3809
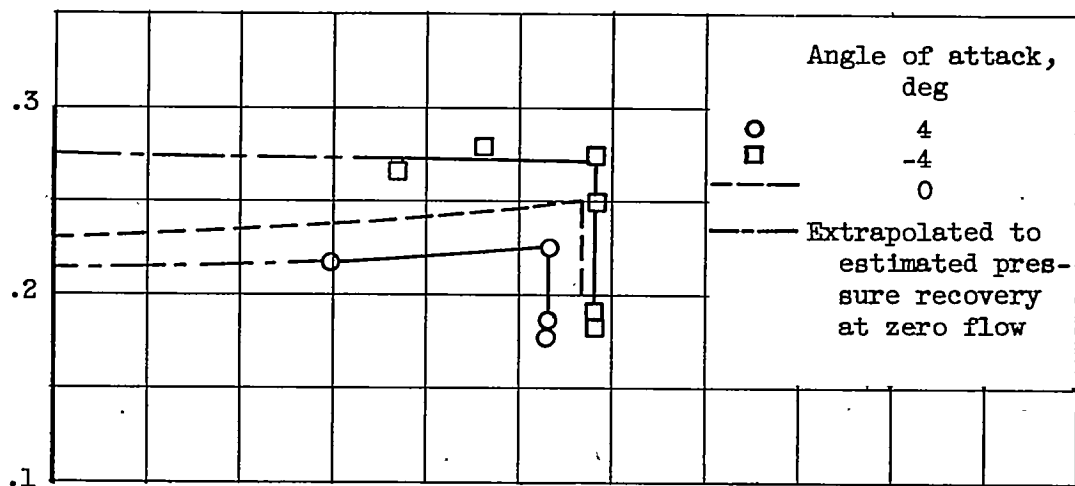
(e) Inlet 0.324.
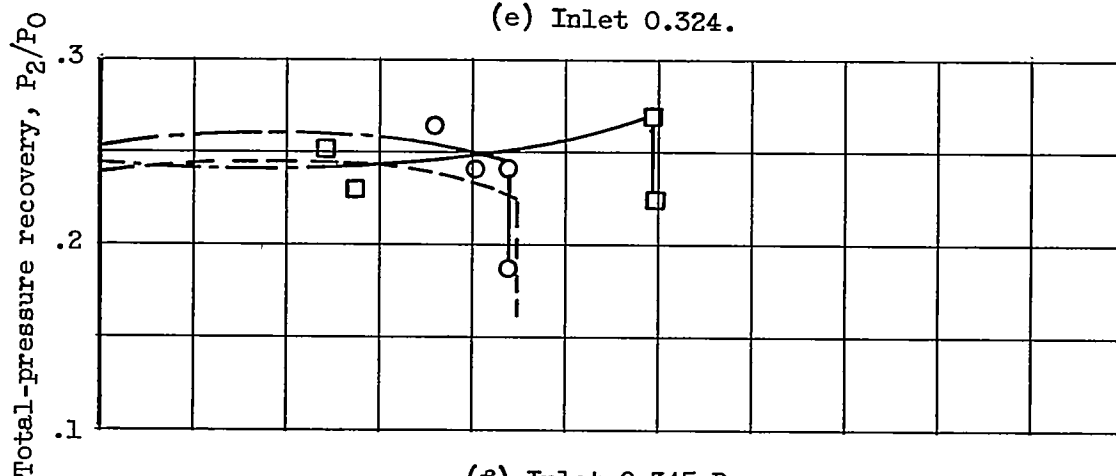
(f) Inlet 0.345-D.
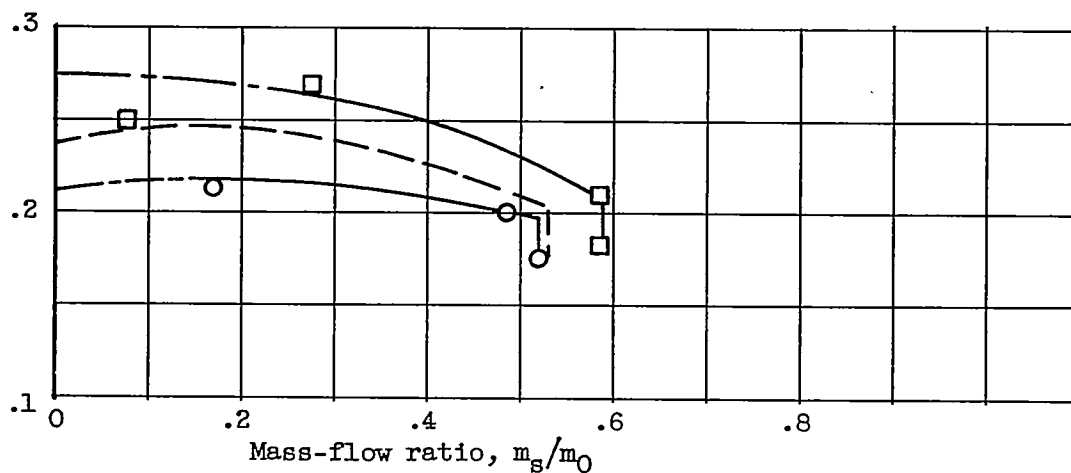
(g). Inlet 0.239.

Figure 8. - Continued. Effect of angle of attack on inlet per-
formance characteristics; free-stream Mach number, 2.0.
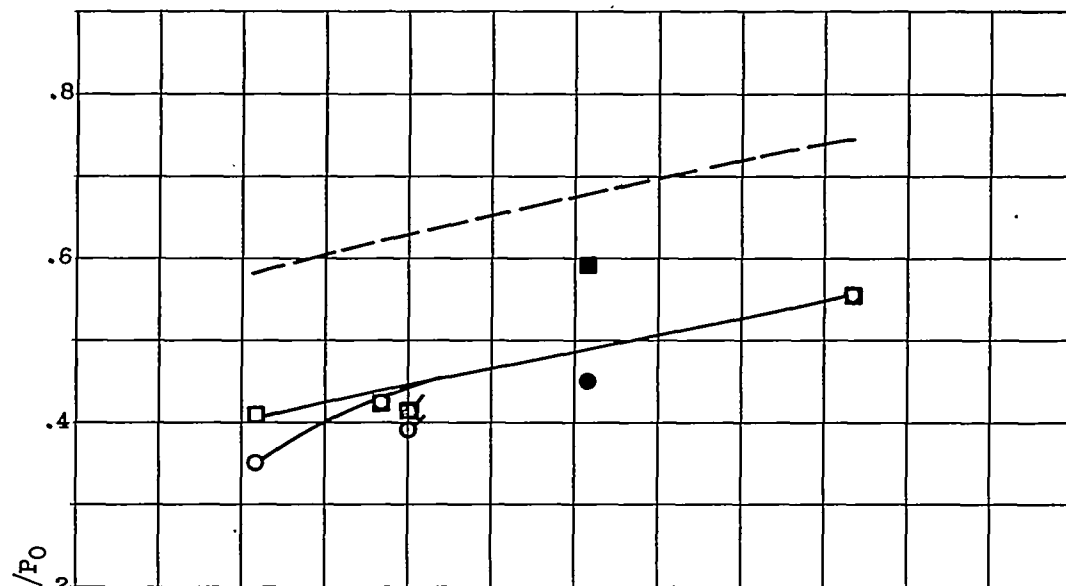
(a) Free-stream Mach number, 1.5.
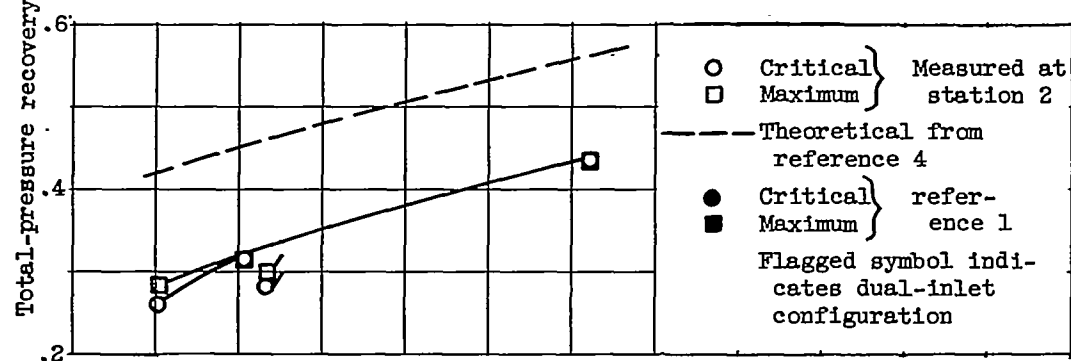
(b) Free-stream Mach number, 1.8.
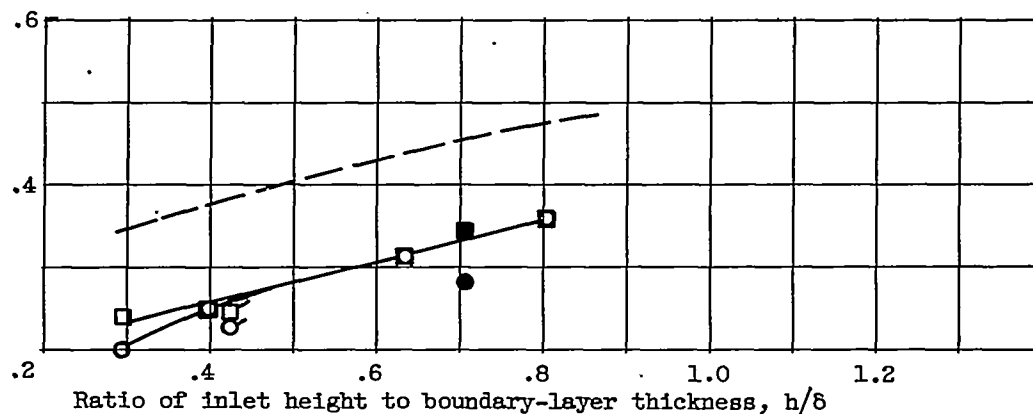
(c) Free-stream Mach number, 2.0.

Figure 9. - Effect of inlet boundary-layer immersion on pressure recovery at zero angle of attack.

(a) Inlet 0.239; critical operating point; total-
pressure recovery, 0.200.

(b) Inlet 0.324; critical operating point; total-
pressure recovery, 0.252.

(c) Inlet 0.512; critical operating point; total-
pressure recovery, 0.315.
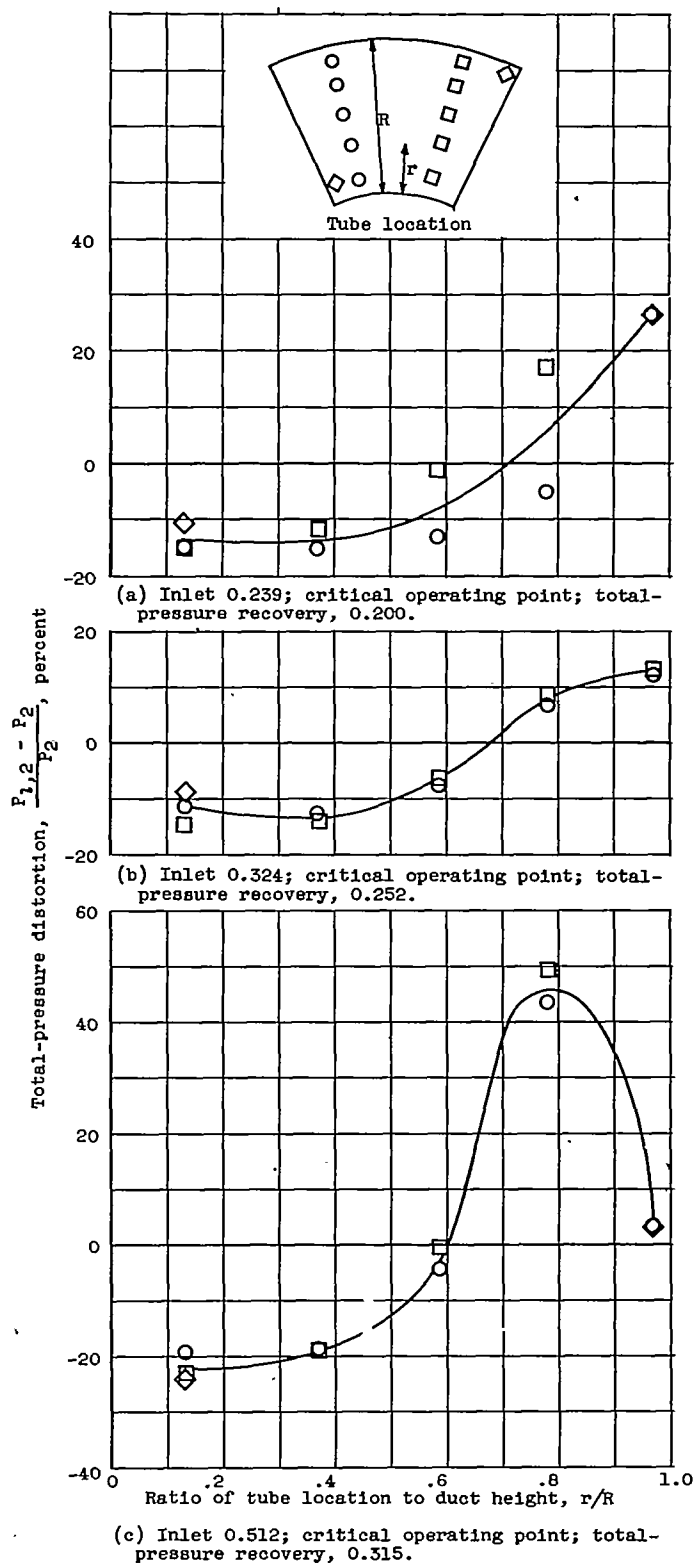
Figure 10. - Effect of inlet height on total-pressure
distortion at inlet-discharge station; free-stream
Mach number, 2.0; zero angle of attack.
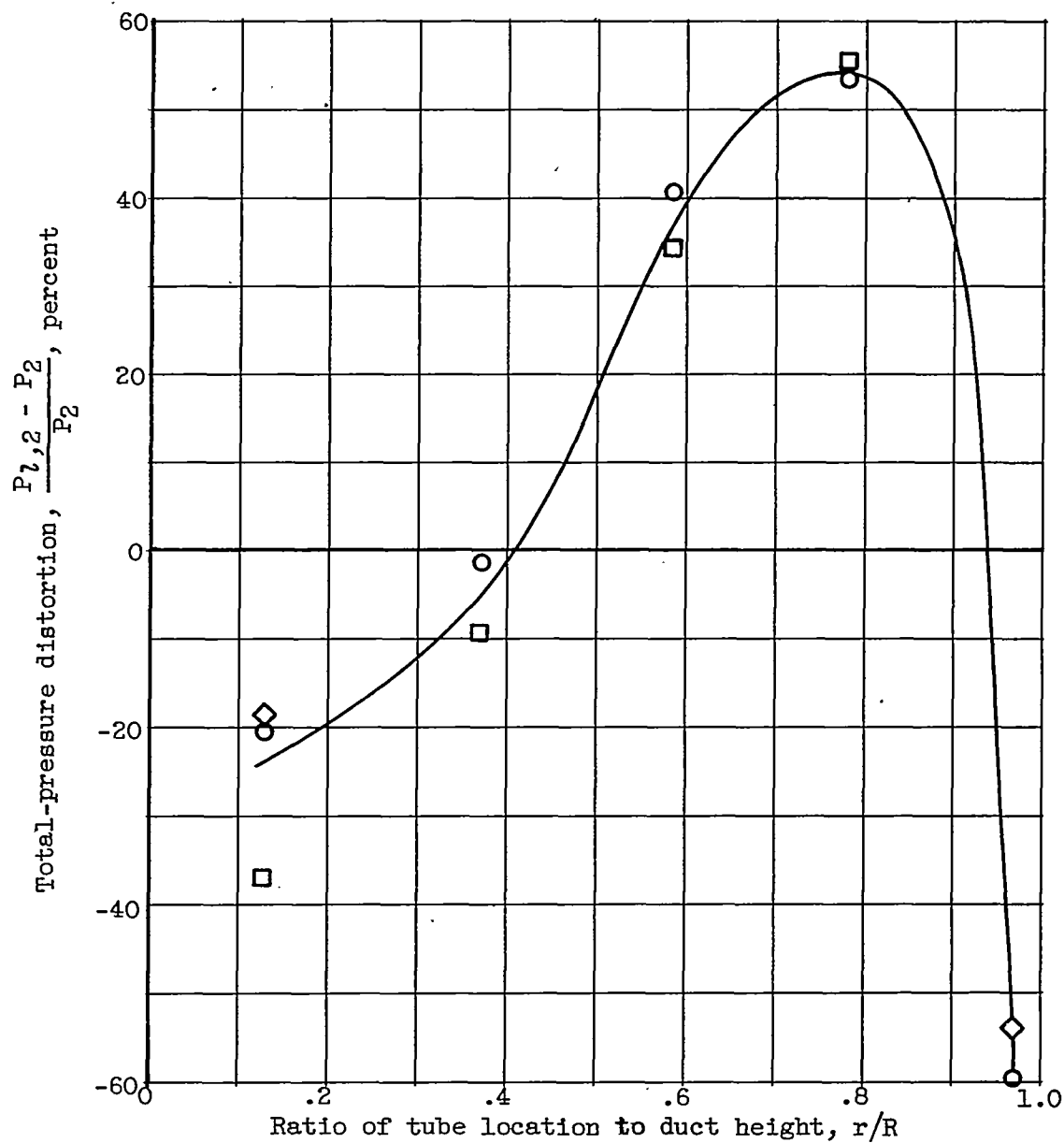
(d) Inlet 0.653; critical operating point; total-pressure recovery, 0.355.

Figure 10. - Concluded. Effect of inlet height on total-pressure distortion at inlet-discharge station; free-stream Mach number, 2.0; zero angle of attack.

3809
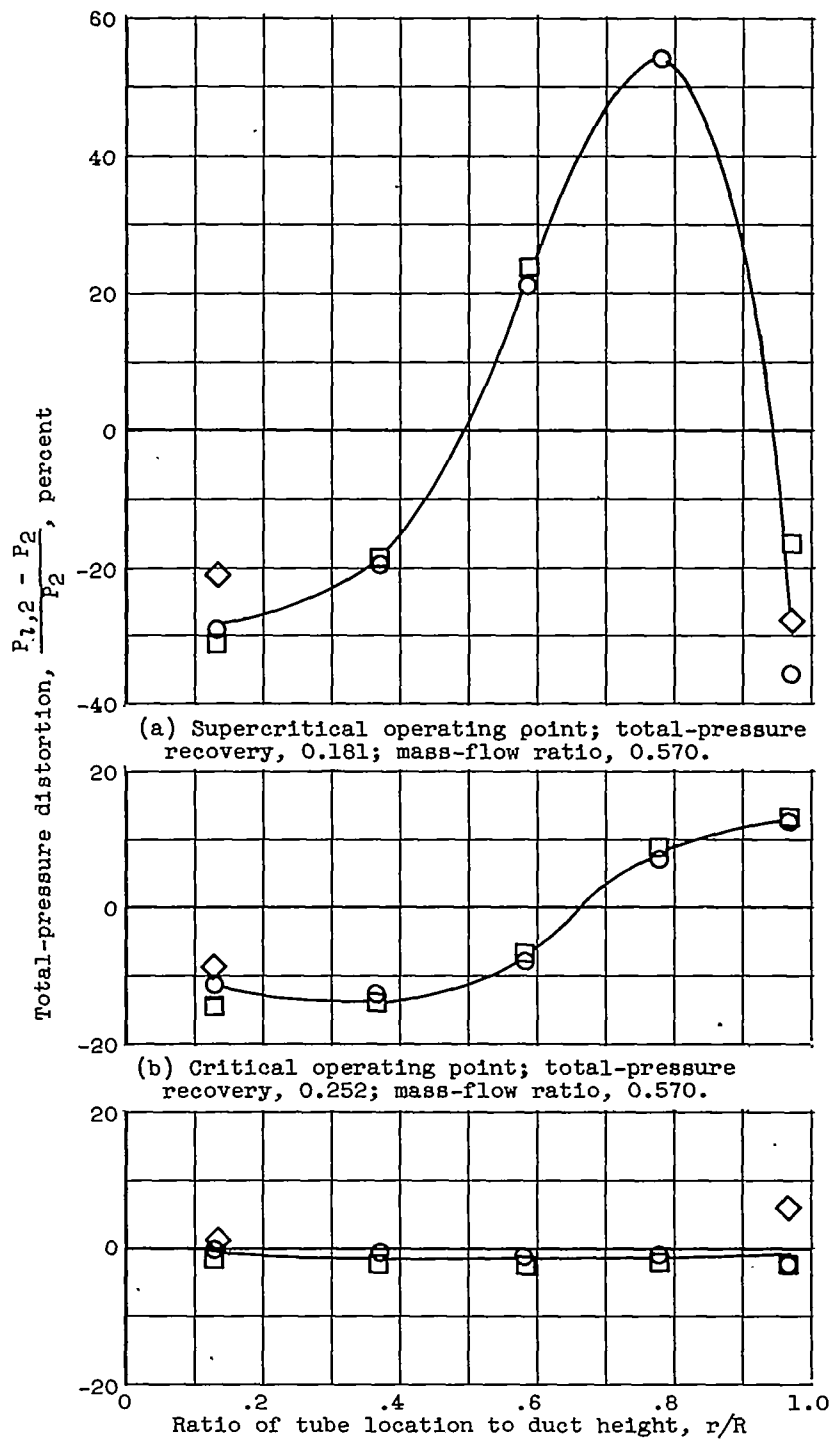
(a) Supercritical operating point; total-pressure
recovery, 0.181; mass-flow ratio, 0.570.

(b) Critical operating point; total-pressure
recovery, 0.252; mass-flow ratio, 0.570.

Ratio of tube location to duct height, r/R

(c) Subcritical operating point; total-pressure
recovery, 0.235; mass-flow ratio, 0.206.

Figure 11. - Effect of inlet operating condition
on total-pressure distortion at inlet-discharge
station; inlet 0.324; free-stream Mach number,
2.0; zero angle of attack.

(a) Mass-flow ratio, 0.663; supercritical operation.

(b) Mass-flow ratio, 0.712; supercritical operation.

(c) Mass-flow ratio, 0.686; critical operation.

(d) Mass-flow ratio, 0.134; subcritical operation.
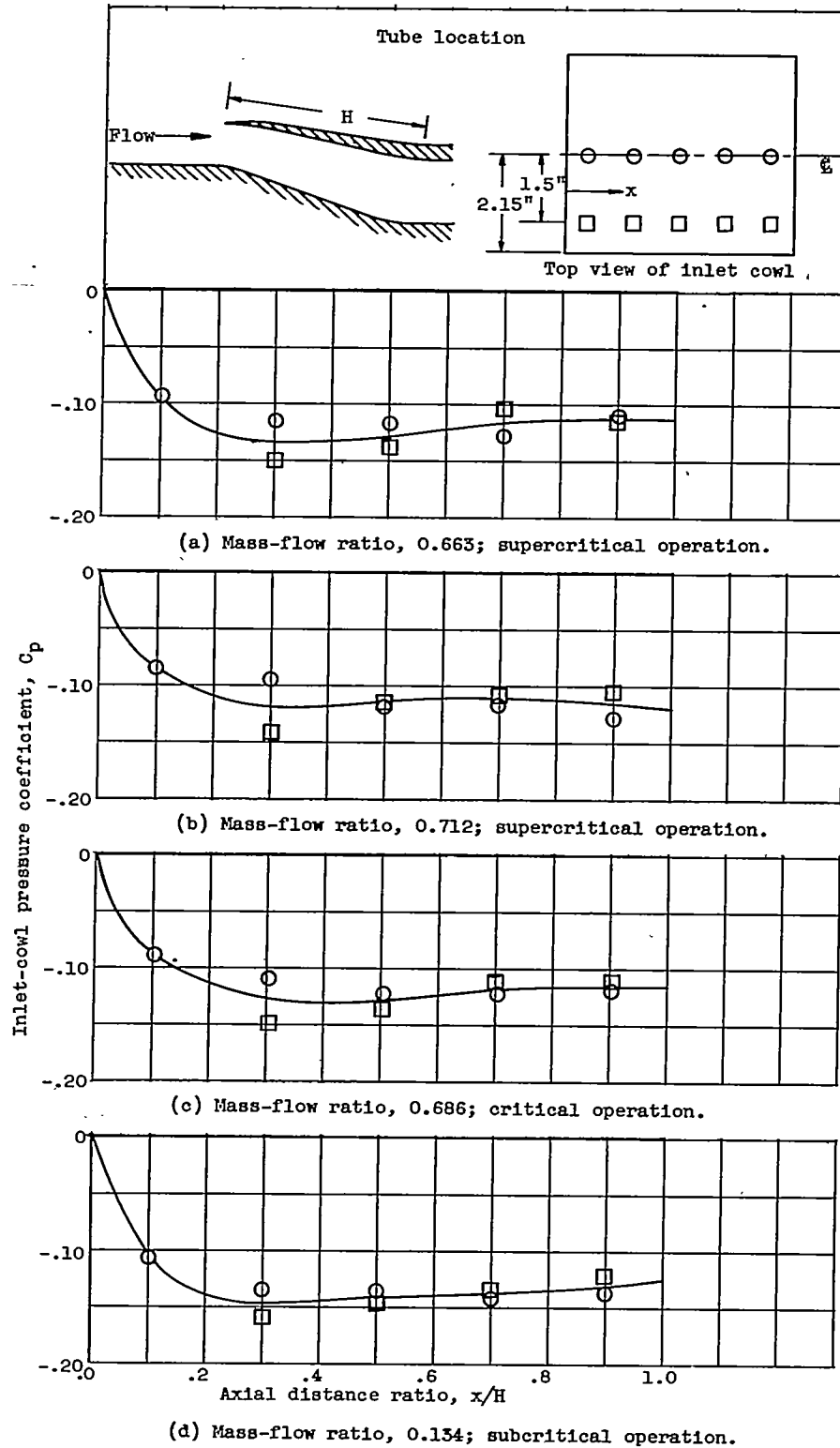
Figure 12. - Representative external pressure distributions on the inlet cowl. Inlet 0.653 at free-stream Mach number, 2.0; zero angle of attack.

(a) Free-stream Mach number, 2.0.

(b) Free-stream Mach number, 1.8.

(c) Free-stream Mach number, 1.5.

(d) Free-stream Mach number, 0.64.
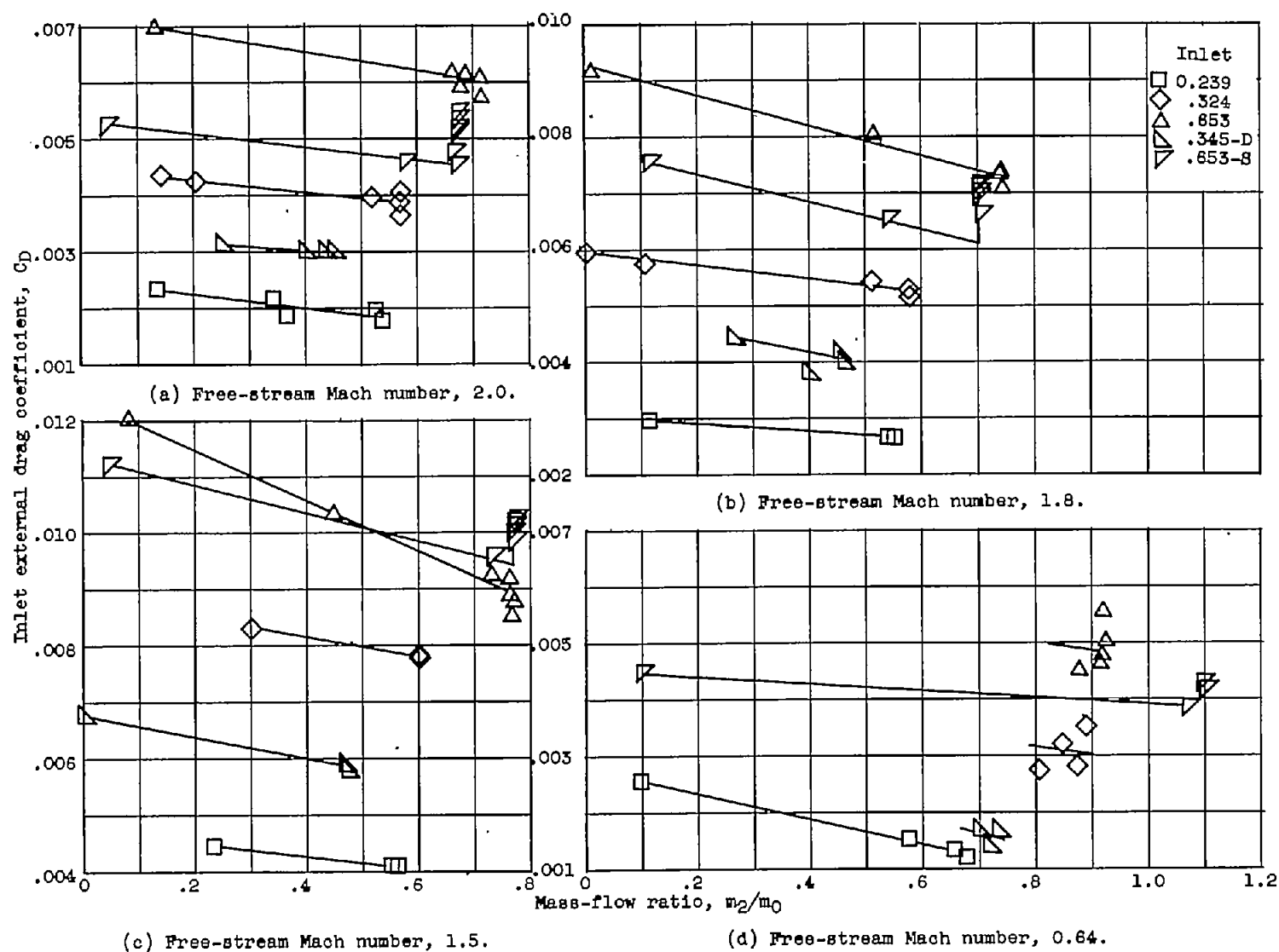
Figure 13. - External pressure drag of auxiliary inlets; zero angle of attack.
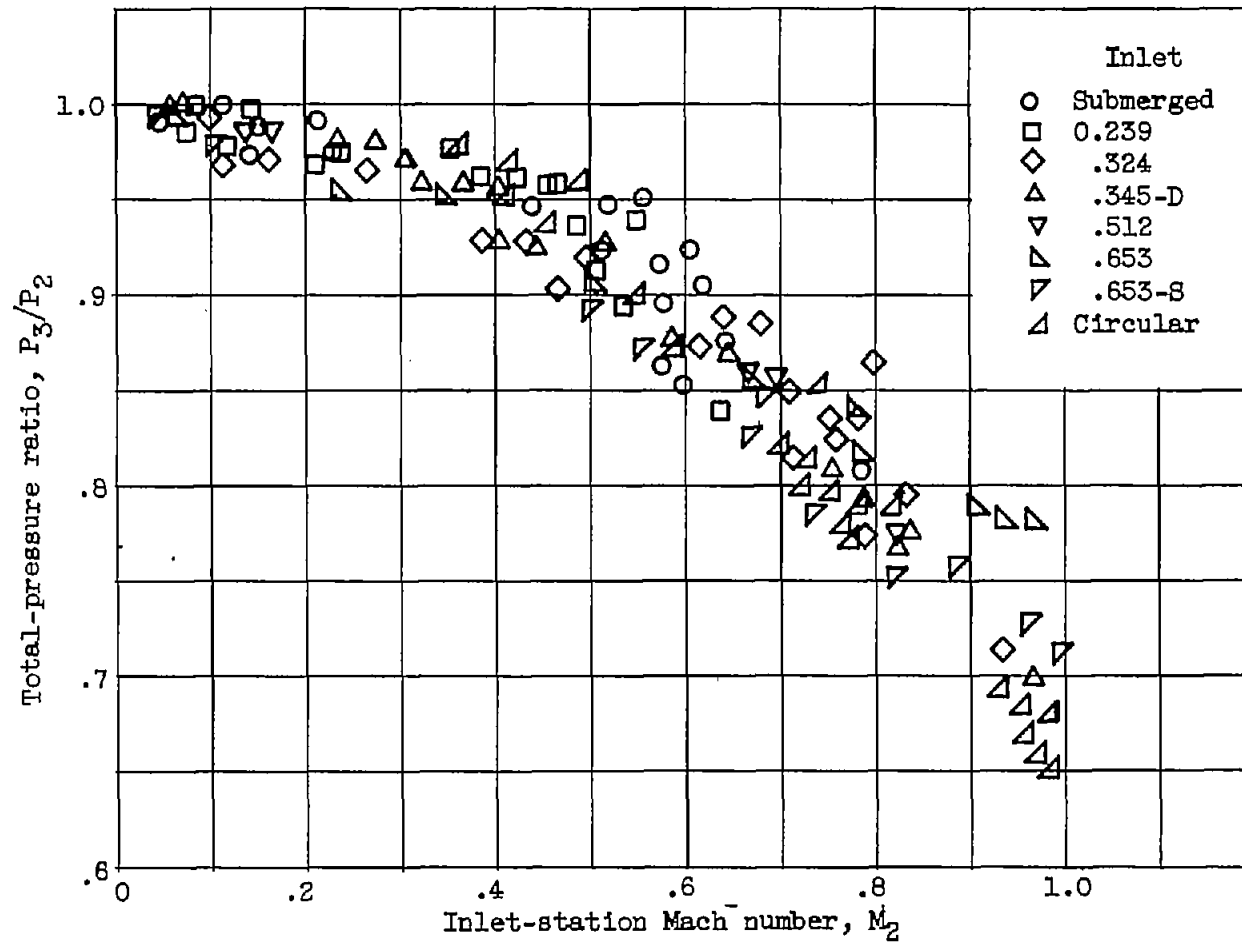
Figure 14. - Effect of Mach number at inlet station on ducting losses to nozzle station.
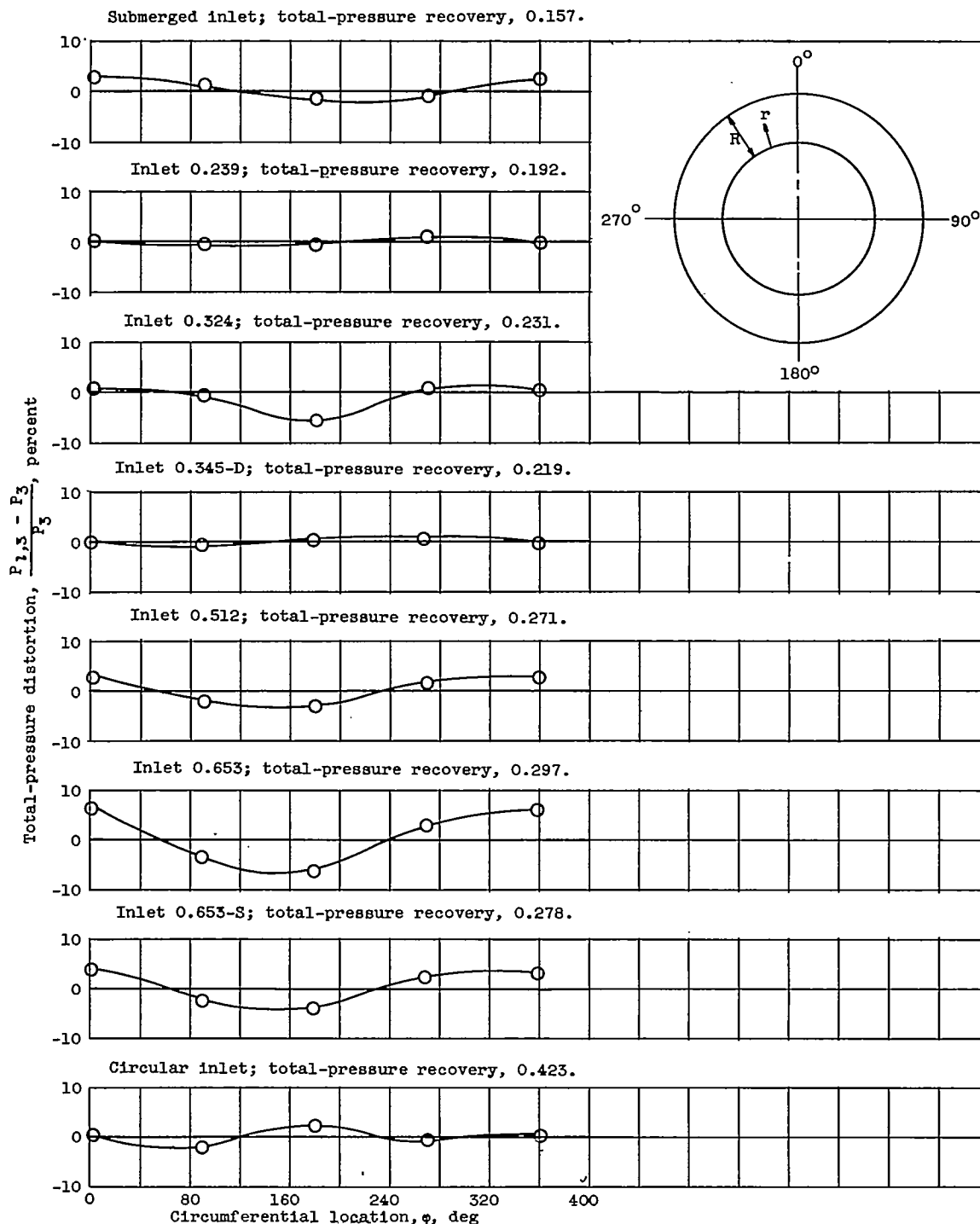
(a) Circumferential profiles for various inlets operating critically; r/R, 0.5.

Figure 15. - Radial and circumferential total-pressure profiles at nozzle station; free-stream Mach number, 2.0; zero angle of attack.
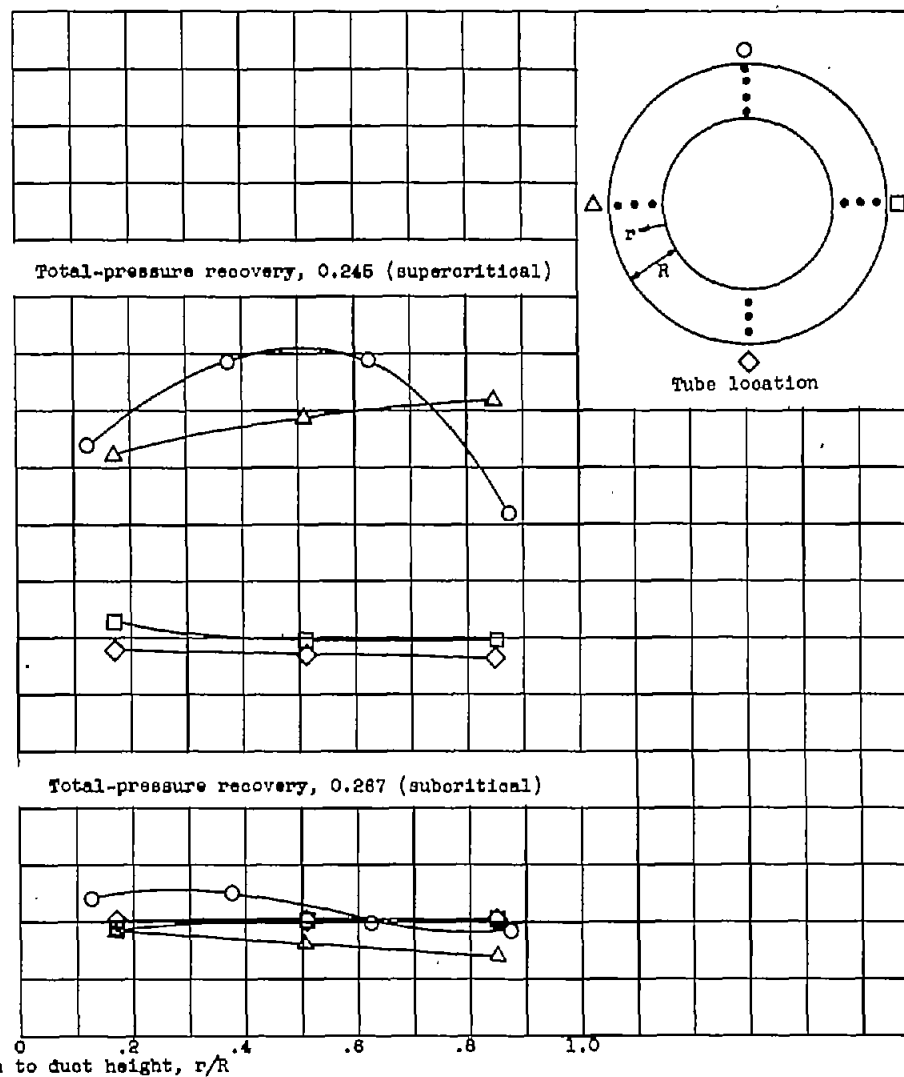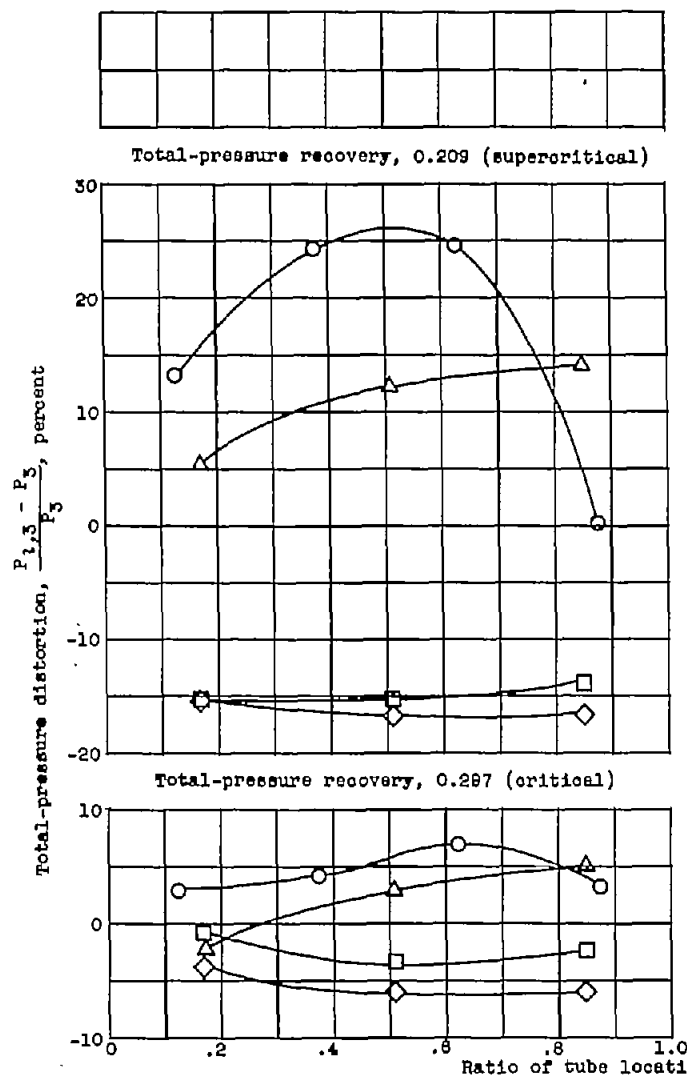
(b) Effect of inlet operating condition on radial profiles; inlet 0.853.

Figure 15. - Continued. Radial and circumferential total-pressure profiles at nozzle station; free-stream Mach number, 2.0; zero angle of attack.

	Total-pressure recovery, P_3/P_0	Inlet-operating conditions
O	0.209	Supercritical
□	.245	Supercritical
◇	.297	Critical
△	.267	Subcritical
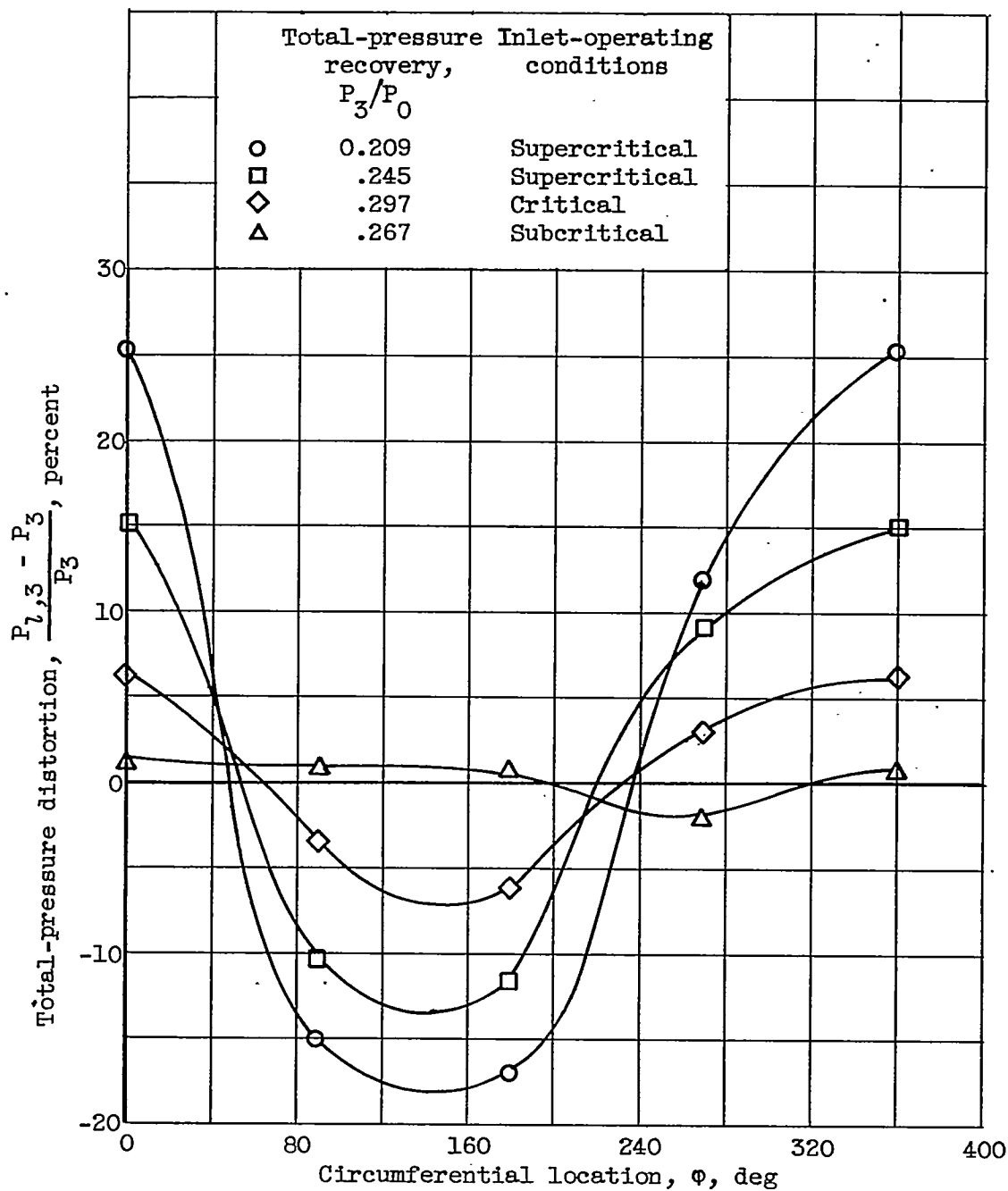
(c) Effect of inlet operating condition on circumferential profiles; inlet 0.653; r/R, 0.5.

Figure 15. - Concluded. Radial and circumferential total pressure profiles at nozzle station; free-stream Mach number, 2.0; zero angle of attack.
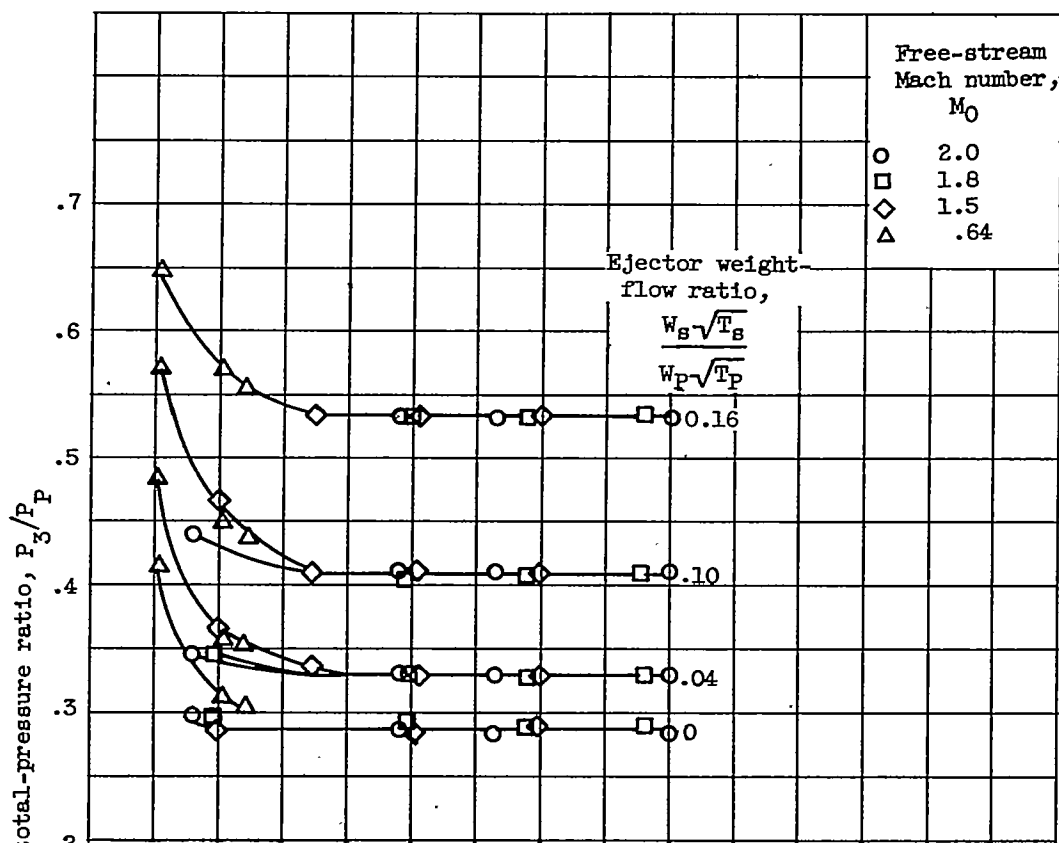
(a) Ejector 1.16-0.80.
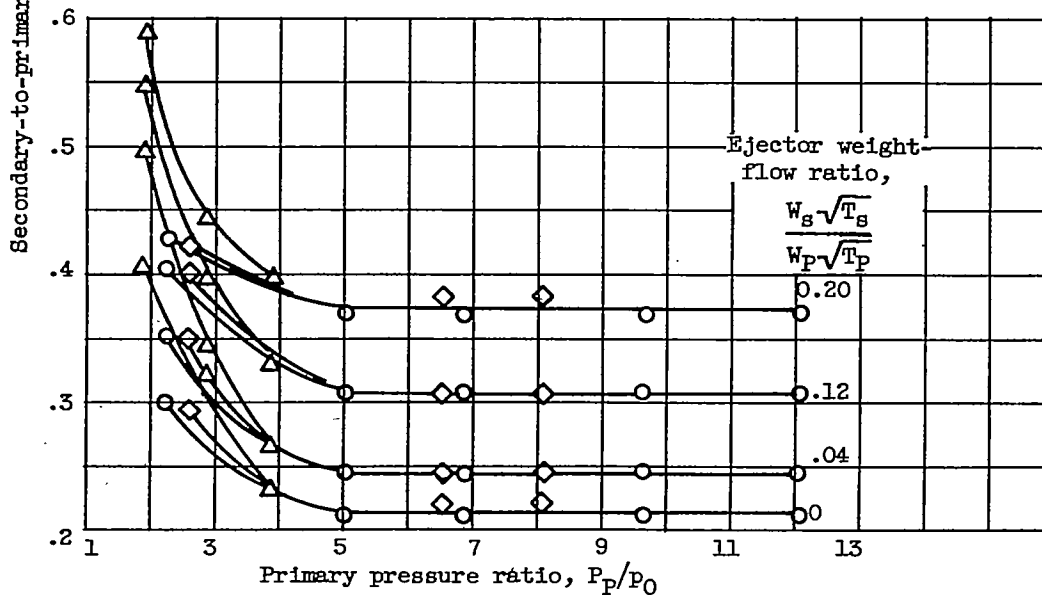
(b) Ejector 1.30-0.80.

Figure 16. - Ejector pumping characteristics showing free-stream Mach number effect.
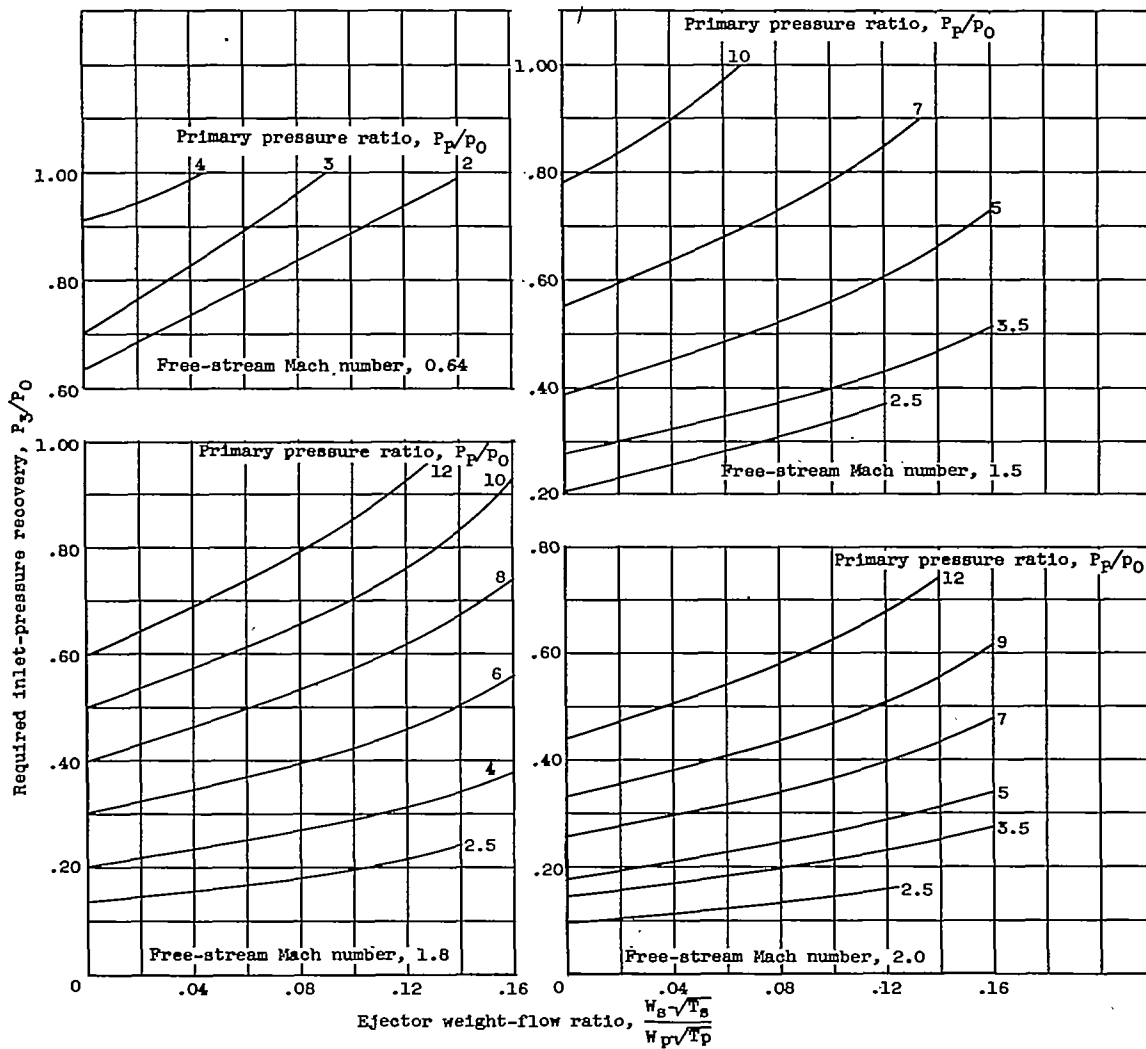
(a) Ejector 1.16-0.80.

Figure 17. - Ejector pressure-recovery requirements.

(b) Ejector 1.30-0.80.
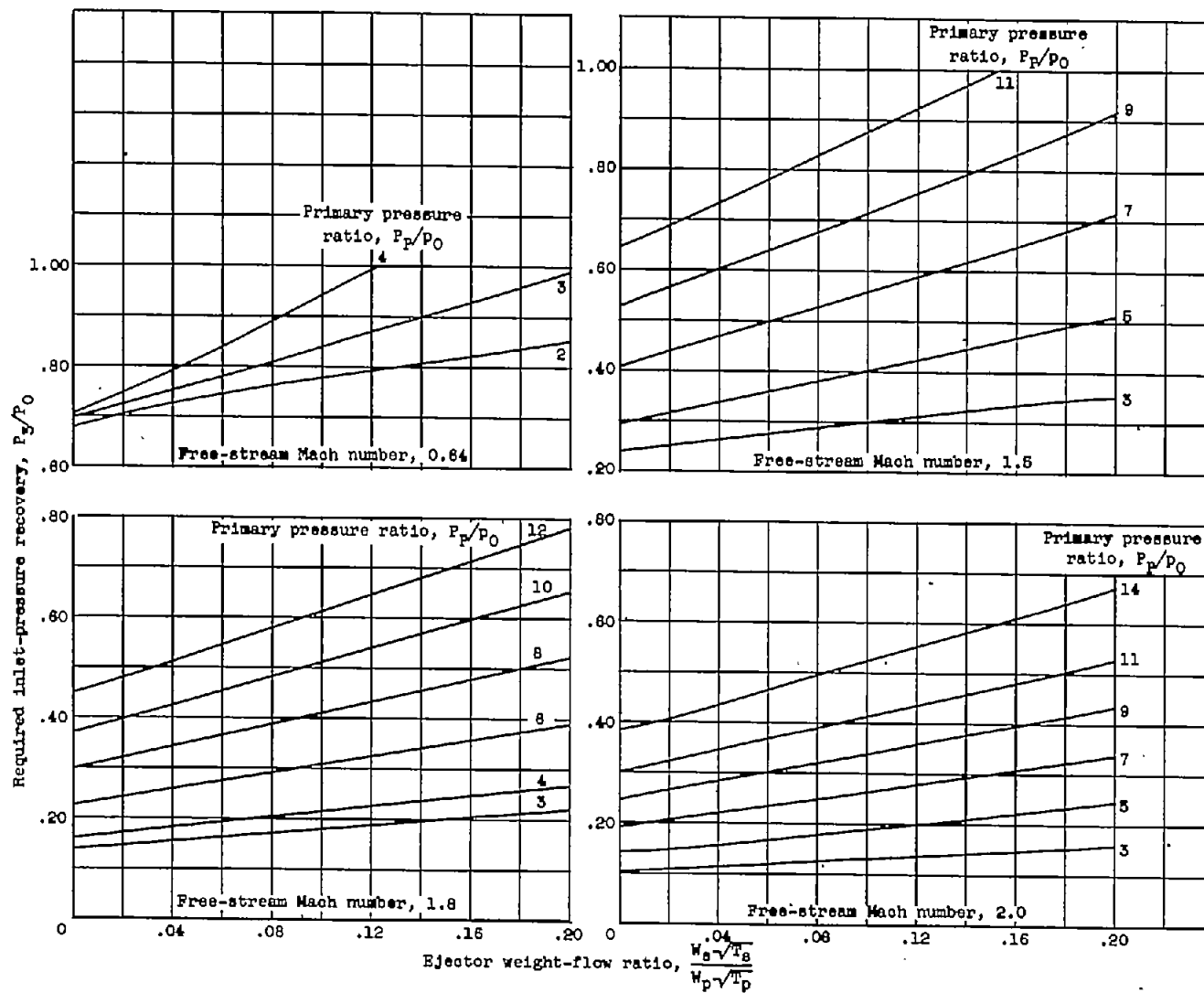
Figure 17. - Concluded. Ejector pressure-recovery requirements.
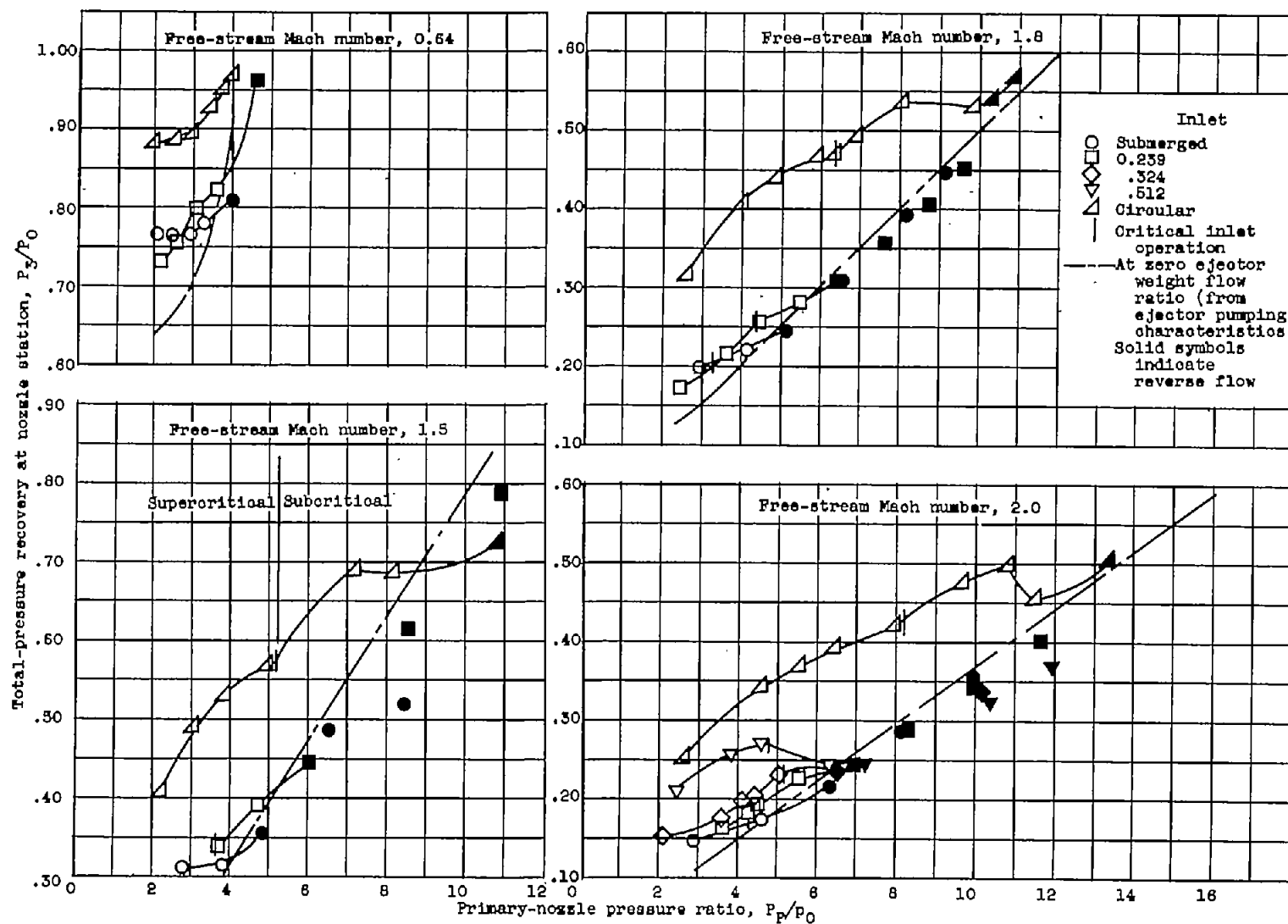
(a) Ejector 1.16-0.80.

Figure 18. - Effect of primary nozzle operation on pressure recovery delivered by inlets; zero angle of attack.
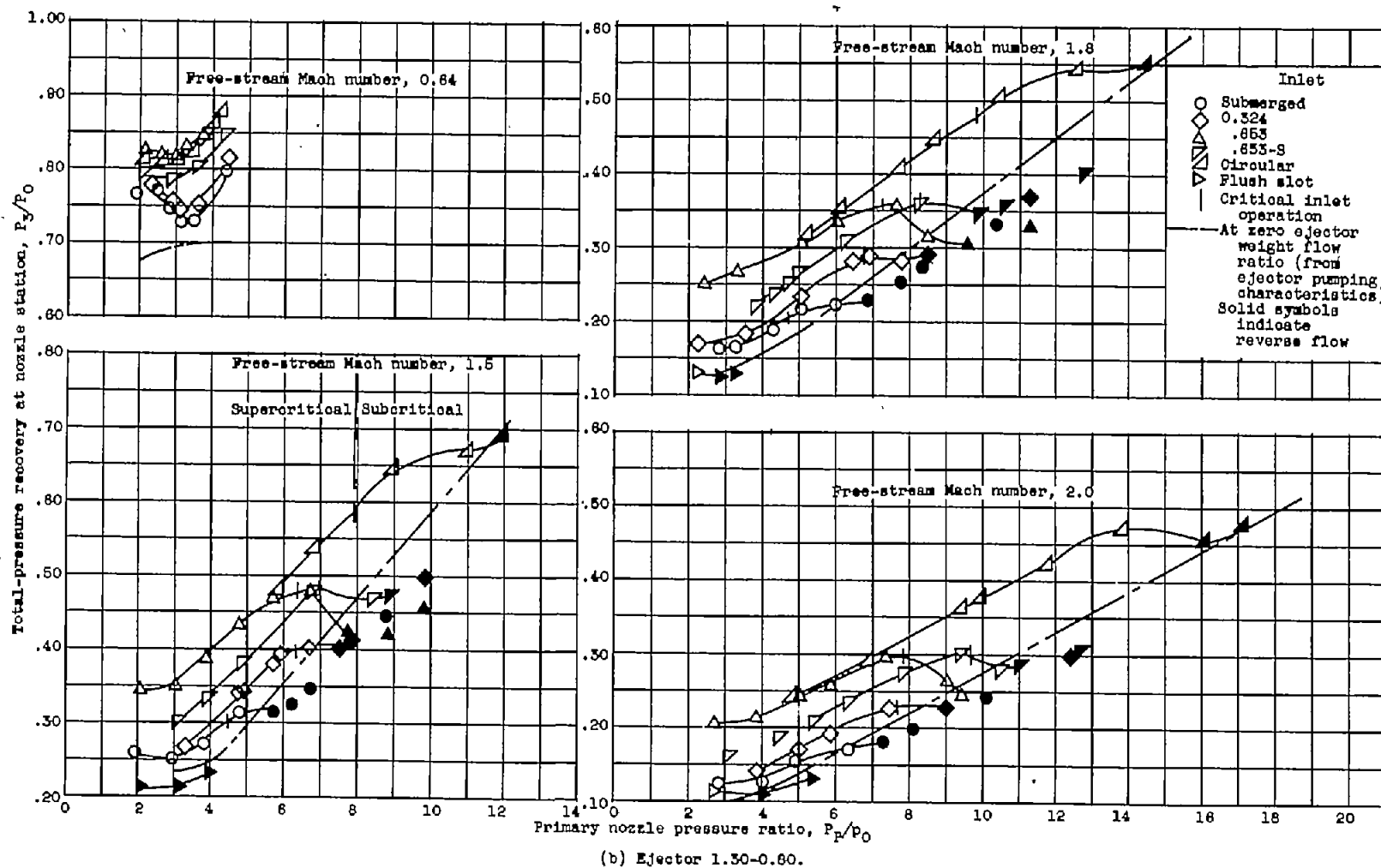
(b) Ejector 1.30-0.80.

Figure 18. - Concluded. Effect of primary nozzle operation on pressure recovery delivered by inlets; zero angle of attack.
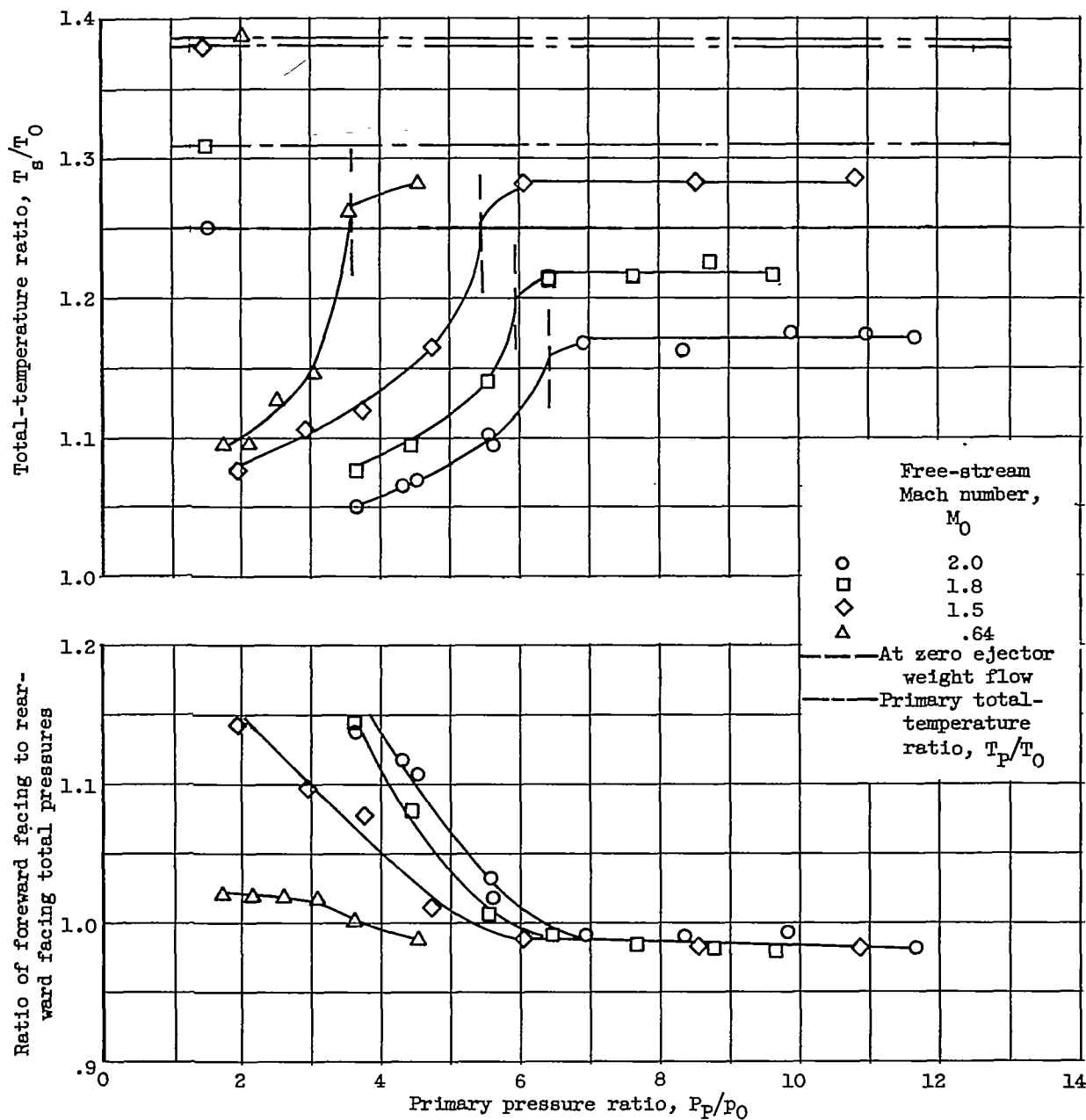
3809

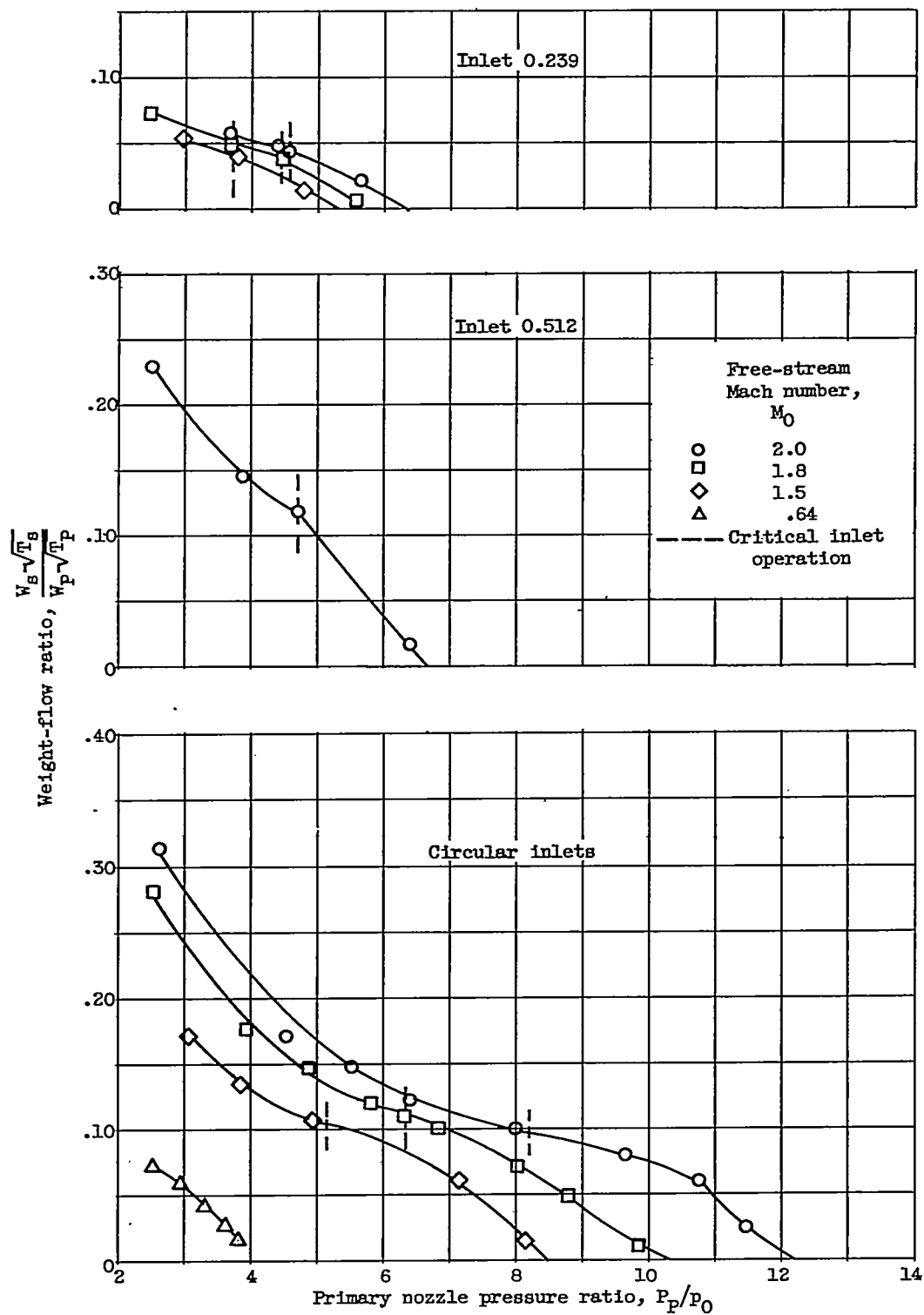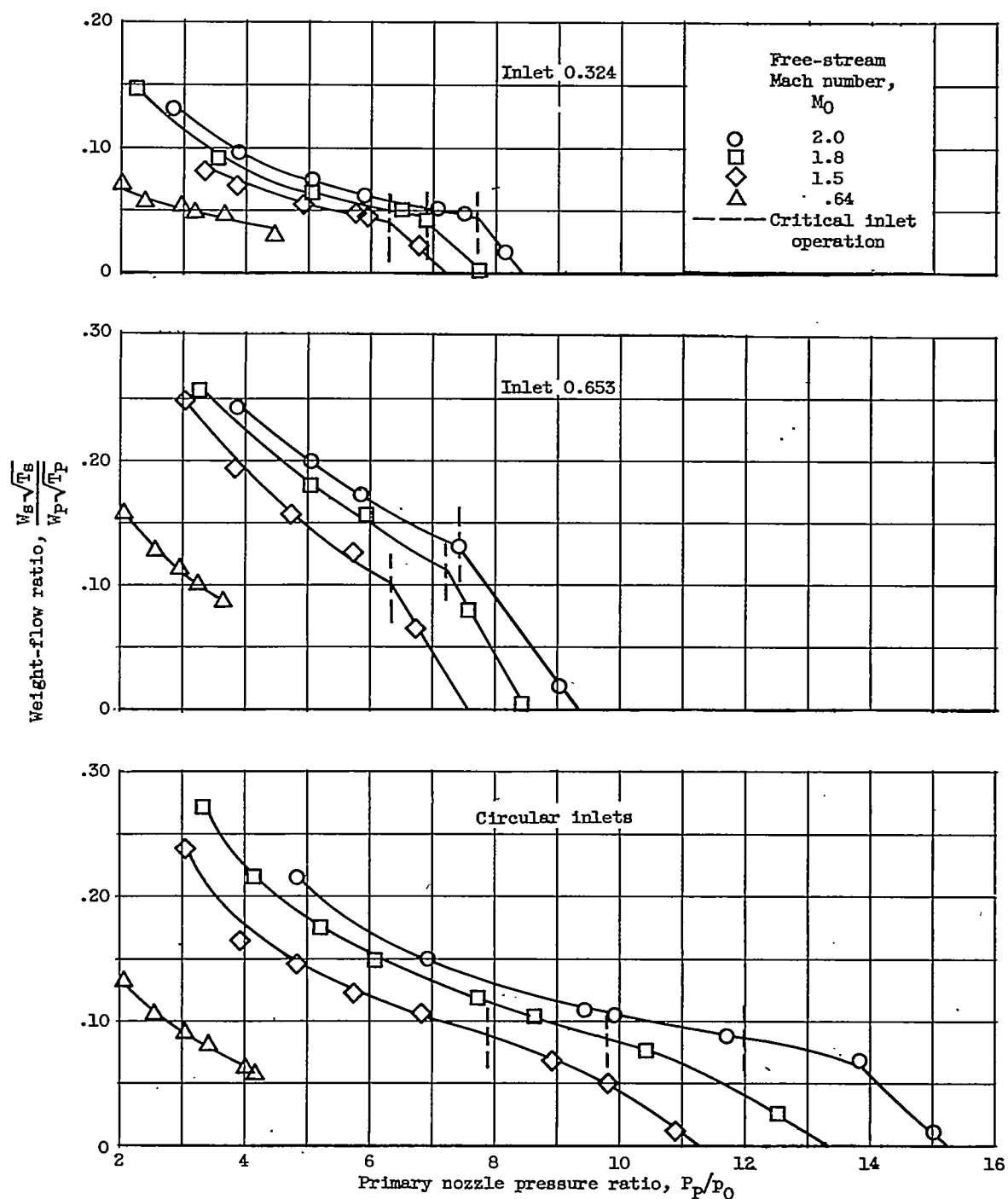Figure 19. - Example of reverse flow determination; inlet 0.239 with ejector 1.16-0.80.

(a) Ejector 1.16-0.80.

Figure 20. - Effect of primary-pressure ratio on ejector weight flow.

(b) Ejector 1.30-0.80.

Figure 20. - Concluded. Effect of primary pressure ratio on ejector weight flow.

(a) Inlet 0.239.

(b) Inlet 0.512.

(c) Inlet 0.324.

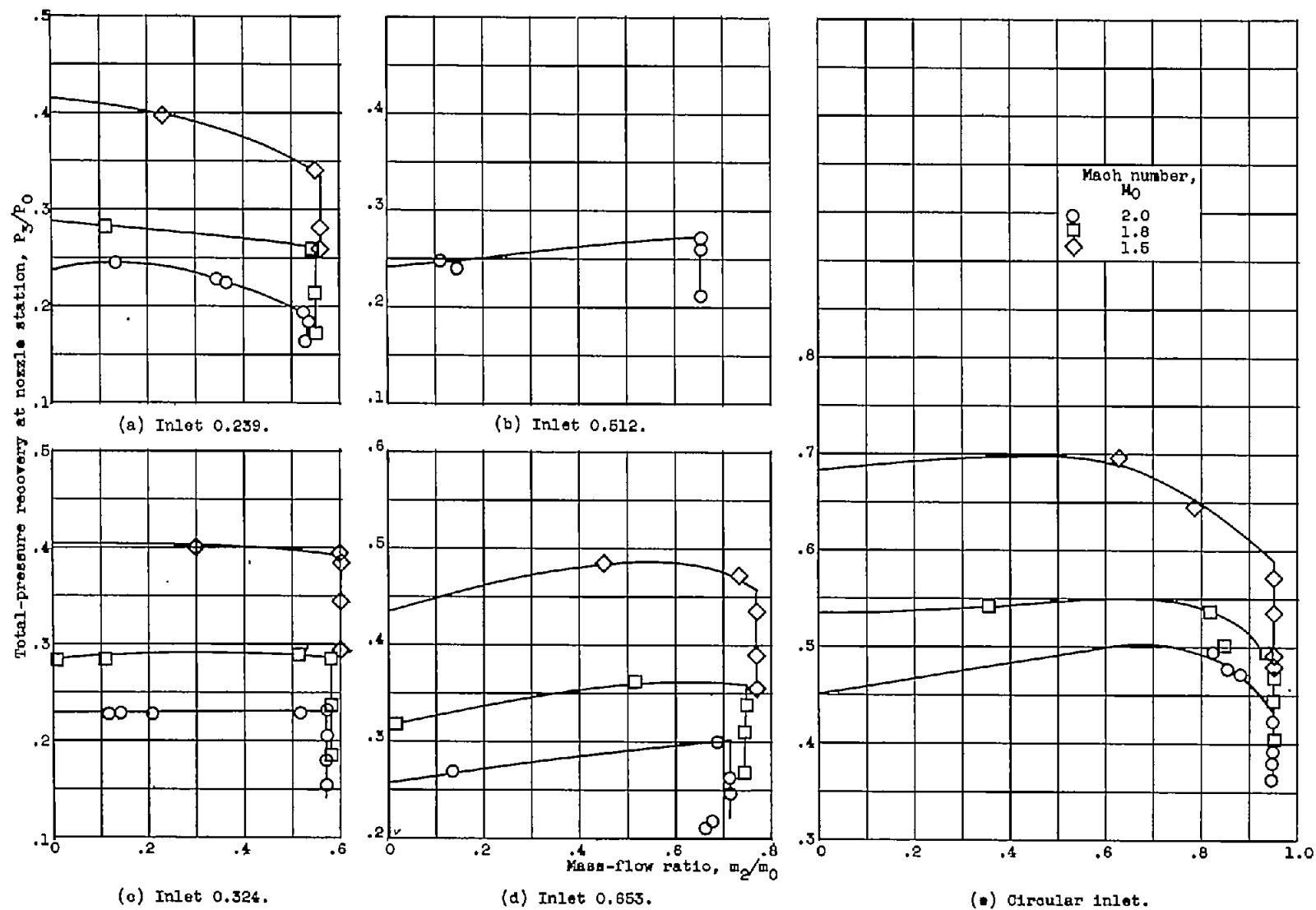(d) Inlet 0.653.

(e) Circular inlet.

Figure 21. - Auxiliary-inlet performance at nozzle station; zero angle of attack.
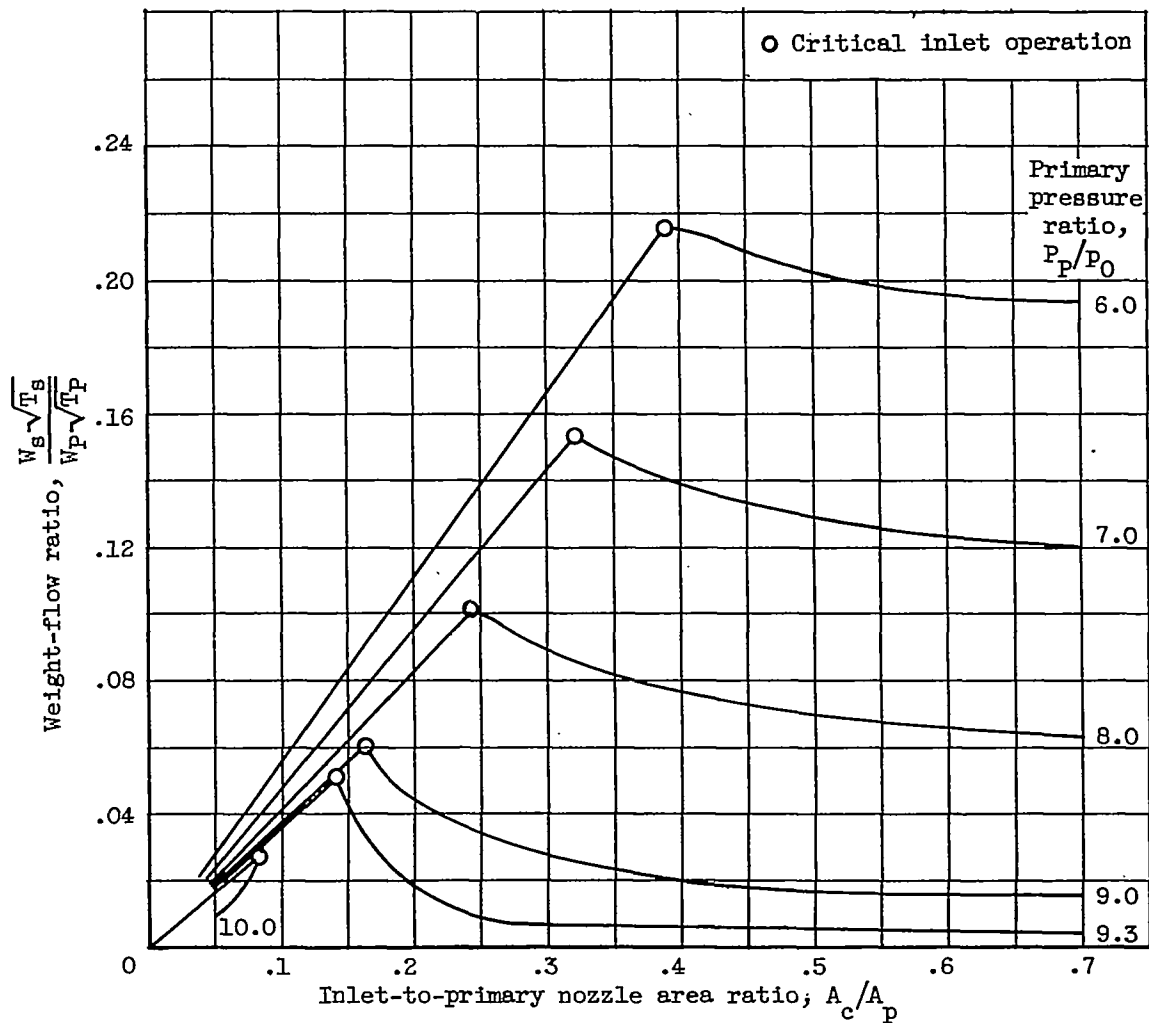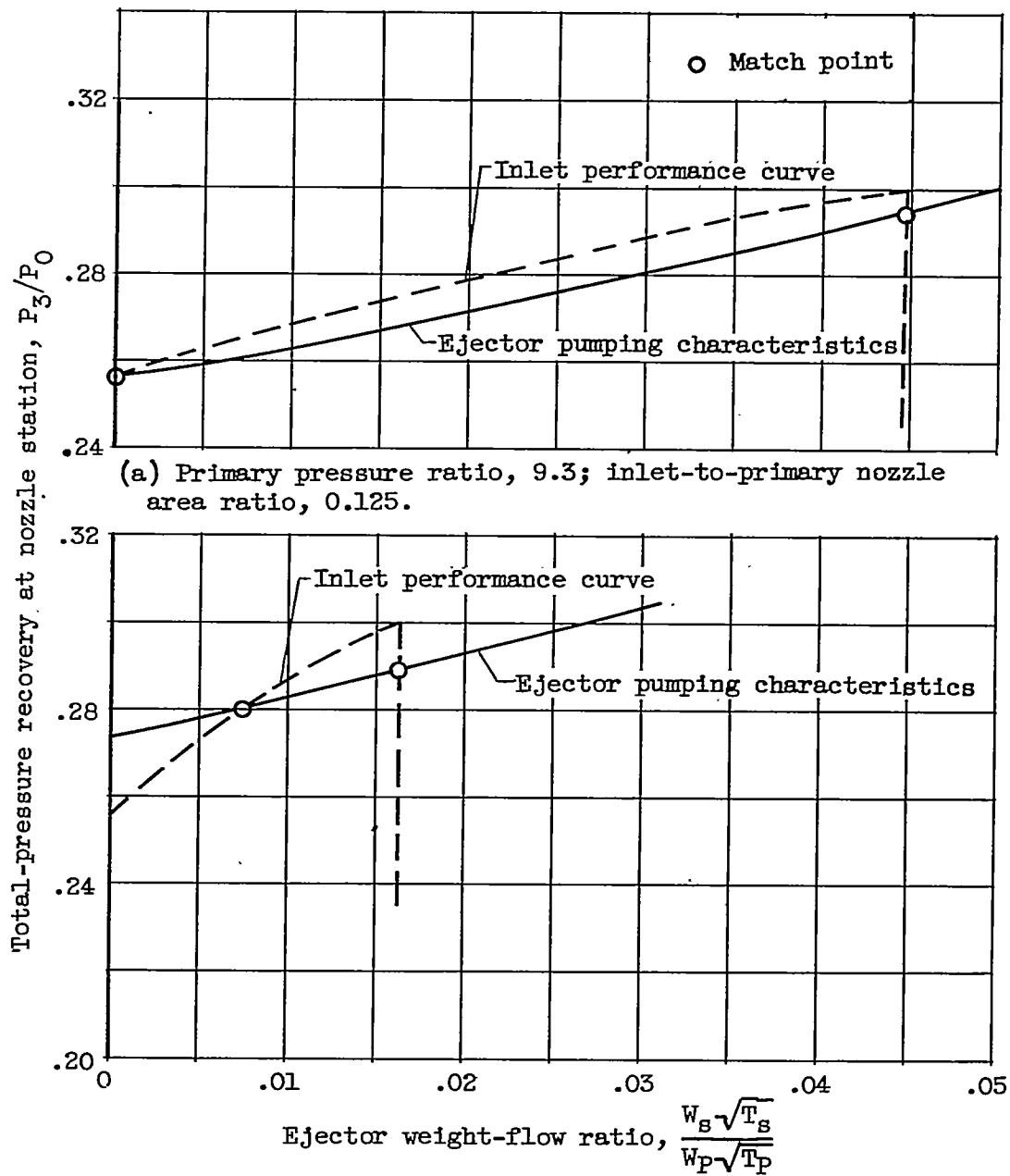
3809

Figure 22. - Effect of inlet size on match point showing effect of
primary-pressure ratio; inlet 0.653, ejector 1.30-0.80; free-
stream Mach number, 2.0; reverse-flow limit at primary-pressure
ratio, 9.3.

(a) Primary pressure ratio, 9.3; inlet-to-primary nozzle
    area ratio, 0.125.

(b) Primary pressure ratio, 10.0; inlet-to-primary nozzle
    area ratio, 0.050.

Figure 23. - Superimposed inlet and ejector maps showing two
    match points; inlet 0.653, ejector 1.30-0.80; free-stream
    Mach number, 2.0.